Evaluation of future temperature and precipitation projections in Morocco using the ANN-based multi-model ensemble from CMIP6

Veysel Gumus[1,2*], Nabil El Moçayd[3], Mehmet Seker[1], Mohammed Seaid[2]

May 18, 2023

[1] Civil Engineering Department, Harran University, Sanliurfa, Turkey
[2] Department of Engineering, University of Durham, South Road, DH1 3LE, UK
[3] International Water Research Institute (IWRI) - Institute of Applied Physics (IAP), University Mohammed VI Polytechnic, Benguerir, Morocco
[*] Correspondence to: Veysel Gumus (gumus@harran.edu.tr)

Abstract

In present study, values of minimum temperature, maximum temperature and precipitation at 27 observation stations in Morocco are used to implement an artificial neural network based downscaling approach in order to simulate regional climate and to investigate the impact of climate change on the country under different scenarios. For this purpose, the best models representing the country among the 15 GCMs within the scope of the CMIP6 are first identified. Then, using the artificial neural network based statistical downscaling method, a multi-model ensemble is created for each climate parameter. Following the performance evaluation based on different statistical metrics and their aggregated values, a good agreement between the observed and the predicted variables is achieved. This allows us to assess future projections of temperature and precipitation following two climate scenarios, namely the SSP2-4.5 and SSP5-8.5. Spatial as well as temporal changes are evaluated for three different time periods namely, 2025-2049, 2050-2074 and 2075-2100. Both scenarios indicate that an important increase of the minimum and maximum temperatures is expected and it can reach up to 5 °C by the end of the century in some regions of the country. Seasonal variability has also been addressed here under climate change scenarios, and consistent variations with annual changes are also reported during each season, except for the summer where the increase barely goes beyond 1.5 °C. The current analysis also includes the variation of precipitation at both seasonal and annual timescales. The country is likely to experience an important drought during the upcoming years, reaching a decrease of roughly 30% and 50% each year

respectively, under the SSP2-4.5 and SSP5-8.5 scenarios by the end of the century. This change is also consistent over the seasons, especially during fall, winter and spring seasons, when Morocco receives its major amount of precipitation.

Keywords: Climate change, Temperature, Precipitation, Projections, CMIP6, Artificial neural network

1 Introduction

Morocco, being part of the Mediterranean region, is one of the most vulnerable countries to climate change (Schilling et al., 2012). Based on many global climate models (GCMs) that have simulated future scenarios in the region, an important increase in temperature and an intense decrease in precipitation are expected (Almazroui et al., 2020). Following these changes, this may alter many sensitive vital economic sectors in the country such as water (El Moçayd et al., 2020) and agriculture (Abdelmajid et al., 2021). Moreover, as another undesired consequence of global changes, many natural disasters are expected to be more and more recurrent following the occurrence of extreme weather events such as heavy precipitation (Tramblay et al., 2012), long drought periods (Zkhiri et al., 2019) and large episodes of heatwaves (Khomsi et al., 2018). These events would have negative impacts on the resilience of emerging cities (Satour et al., 2021) and human health (Habib et al., 2010) among others. Consequently, the overall development of the country will be largely impacted and its pace will be slowed down. Yet, the intensity of this change remains still subject to ubiquitous uncertainties and building reliable adaptation strategies that can cope with these changes are therefore very challenging (Hallegatte, 2009). **In general, the climate in Morocco is characterised by considerable spatio-temporal variability. This is mainly due to its particular location between the extra-tropics which render the climate sensitive to numerous large scale oscillations. In addition, the country is shaped by substantial topography driven mainly by the presence of Rif and Atlas mountains which greatly impact the dynamics of the local climate (Tuel et al., 2022). Usually, the climate modelling relies on Global Circulation Models (GCMS) which are helpful to describe large scale oscillations under the excitation of various effects such as greenhouse gas emission, human activities, volcanic activities, among others. However, because of the physical parameterization of several physical phenomena, their accuracy is not perfect for every region in the globe. This is particularly true for Morocco where some studies revealed the limitation of those models to accurately capture the dynamics associated with large scale circulations impacting the country, see for instance (Tuel et al., 2021). Still even if global circulation is well represented, climate model can suffer from large uncertainties which can be reduced through downscaling (Gao et al., 2006).**

Dynamical downscaling has received wide attention in Morocco, see for instance (Tuel et al., 2021; Tramblay et al., 2013). This has the advantage of being highly efficient in regions where data records are sparse. Many high-resolution Regional Climate Models (RCMs) have been developed because of this main limitation and they have succeeded in modeling the extremely variable climate in the region. Yet, this approach is not perfect as RCMs suffer also from ubiquitous uncertainties that can be driven from different elements such as the spatial resolution, the bias correction or the boundary description. In fact, choosing a good spatial resolution is a key ingredient in dynamical downscaling that may alter the accuracy of simulations. The first simulations for RCMs in the region used horizontal grid spacing larger than 20 Km, see for example (Tramblay et al., 2013). However, with the growing computational capacities, higher resolutions were possible achieving 13 Km, see (Tuel et al., 2021). This has not only led to reduce the overall observed uncertainty but also to develop a class of comprehensive climate simulations which allowed to further understand the physical mechanisms responsible for the observed variability in the region. Needless to mention that bias correction is also an important driver of the observed uncertainty in RCMs simulations (Ruffault et al., 2014). In fact, these models need a boundary description to perform climate simulations and generally, this information is available in simulations using GCMs. Unfortunately, these simulations are subject to systematic biases that need to be corrected which may lead to unsatisfactory results even with the use of very high-resolution models, and advanced methods for the bias correction as argued by (Tramblay et al., 2013). Indeed, another major drawback of the use of GCMs to force the simulations using RCMs is the limitation displayed by the selection of the right GCMs. This choice needs to be made carefully since the simulation needs to be consistent with the regional climatology. **For example (Tuel et al., 2021) have demonstrated that only three of the CMIP5 in GCMs are able to capture the regional climatology of Morocco using dynamical downscaling and still their ability to simulate complex meteorological events has not been addressed. The statistical downscaling represents an attractive alternative method to dynamical downscaling but, given the limitation of data availability, statistical downscaling has received little attention**. However, with the establishment of new databases in the region (Tuel and El Moçayd, 2023) and with the expansion of machine learning methods, new methodologies based on the Ensemble methods would allow to consider this class of method. In fact, the use of Bagging (multi-model approach) in ensemble-based methods has already been proven to be effective when the size of databases is limited, see for instance (El Moçayd and Seaid, 2021). This has paved the way towards using machine learning (ML) based statistical downscaling, (Sachindra et al., 2018), especially those relying on multi-model ensemble.

Artificial Neural Network (ANN) method among ML techniques is frequently used in simulations of atmospheric variables and has been reported to be a successful method in downscaling studies Okkan and Kirdemir (2016); Hosseini Baghanam et al. (2022); Seker and Gumus (2022). This method has the ability to determine the most complex level of relationship between large-scale GCM outputs and basin-scale climate variables Seker and Gumus (2022).In the present study, a machine learning models based on ANN is trained using historical records of precipitation and temperature variables to downscale multi-model ensemble from the CMIP6. The trained model is then used to evaluate future projections of precipitation, minimum temperature and maximum temperature under different climate change scenarios. The presented paper is organised as follows: in section 2, we first define the study area along with the observation stations and GCMs of CMIP6 used in our analysis. Next, in Section 3, we introduce the procedure proposed in this study, the ANN method and the performance criteria used for the model assessment. Section 4 is devoted to the results obtained from the success of the considered models in representing the region. In this section, we also examine the performance of the GCMs and downscaling techniques. Performance of the multi-ensemble and projection analysis are also included in this section. Discussions on the obtained results for different scenarios are presented in Section 5. Finally, Section 6 summarizes the study with concluding remarks.

2 Study area and data

Morocco is a large country located in the northwest of Africa (see Figure 1) for which this particular location makes local climate under the influence of numerous large scale oscillations. As the west coast of the country is facing the Atlantic Ocean, the climate there is under the influence of North Atlantic Oscillation (NAO) (Knippertz et al., 2003), which impacts the moisture availability and precipitation in Morocco. On the other side, the northern-east side of the country is driven by dynamics of the Mediterranean sea. This is particularly true regarding future projections, where the interaction between land and sea has a major role in rendering the area sensitive to climate change (Tuel and Eltahir, 2020). Recent works have also shed the light on other large-scale excitations responsible for controlling the variability of the climate in the region, such as the Madden-Julian Oscillation (MJO) (Gadouali et al., 2020; Chaqdid et al., 2023). This situation is rendered more complex with the topography shaping the country. Indeed, Morocco is surrounded by the Atlas mountains and the Rif mountains which have a large impact on the variability of temperature and precipitation in the country.

Using measured data instead of reanalysis data in statistical downscaling improves the predictive performance of the models (Manzanas et al., 2015). For this reason, observation stations in Morocco, where the Moroccan agency of meteorology known as Direction Générale de la Météo (DGM) makes regular measurements, are considered in the present study. The characteristics of the stations including their ID and geographical coordinates and long-term averaged values for minimum daily temperature ($\mathrm{T_{min}}$), maximum temperature ($\mathrm{T_{max}}$) and daily precipitation (Prep) are summarized in Table 1. The daily measurements recorded at these stations were transformed into monthly values for statistical downscaling. Monthly averaged minimum and maximum temperatures are calculated by taking the monthly average of daily minimum/maximum temperatures (in $^\circ$ C), while precipitation values are calculated by considering the average of daily measurements (in mm/day). Notice that before using the data, a first cleaning step was necessary. All the stations were included in the present study as none of them had more than 10% of missing data. Moreover, since approximately 8% of the data is missing for the precipitation at the station of SKASBATT TADLA in the measurement data between 1980-2014, it has been completed by a linear regression

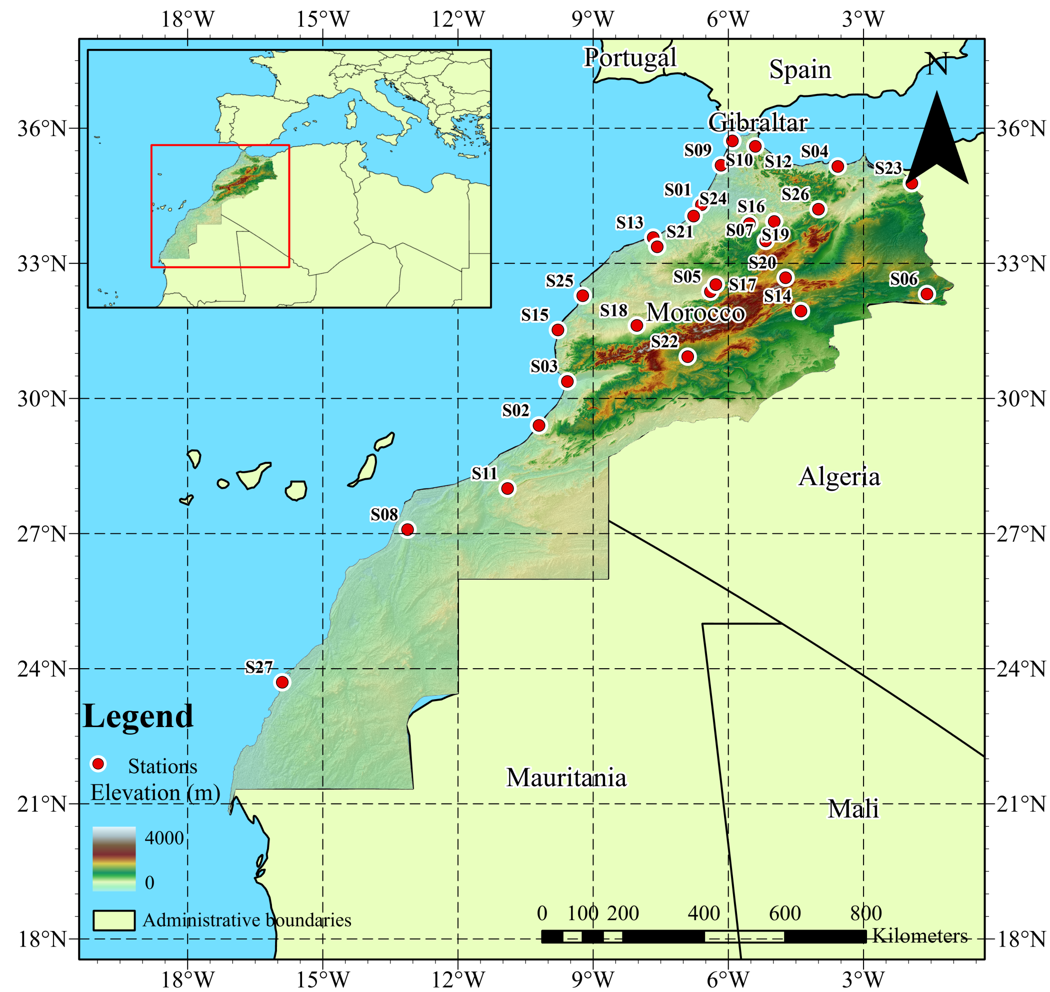

Figure 1: Study area including Morocco's geographical regions considered in the present work. The 27 obesrevation stations are also shown in the map.

from neighbouring stations. For the other historical records data, the highest missing data rate is found to be below 1%.

The CMIP6's 15 GCMs are all selected for analyzing the historical data of monthly averaged daily precipitation, monthly averaged maximum temperature and monthly averaged minimum temperature. These GCMs are provided from the Earth System Grid Federation (ESGF) archive[1]. The institutes, variant labels, and horizontal and vertical resolutions of the GCMs used in the study are listed in Table 2. In order to create a common study concept among the models, it is crucial that they have the same variant (r1i1p1f1). However, different variants are used in four GCMs due to the lack of historical or future data for the variables selected as input to ANN-based downscaling. In addition, since the considered models have different horizontal

[1]https://esgf-node.llnl.gov/search/cmip6

Table 1: Geographical coordinates and mean values of used climate variables of stations considered in this study.

Station ID	Station Name	Longutude (°)	Latitude (°)	T_{min} (° C)	T_{max} (° C)	Prep (mm/day)
S01	KENITRA	-6.60	34.30	13.25	23.12	1.534
S02	SIDI IFNI	-10.20	29.40	16.78	21.89	0.412
S03	AGADIR	-9.57	30.38	14.34	24.09	0.717
S04	ALHOCEIMA	-3.57	35.15	13.93	22.27	0.875
S05	BENI MELLAL	-6.40	32.37	11.24	26.92	0.985
S06	BOUARFA	-1.59	32.32	11.98	24.74	0.437
S07	IFRANE	-5.17	33.50	6.21	18.16	2.648
S08	LAAYOUNE	-13.12	27.09	15.97	26.43	0.155
S09	LARACHE	-6.16	35.18	13.62	22.31	1.881
S10	TANGIER	-5.91	35.72	13.69	22.48	1.886
S11	TANTAN	-10.90	28.00	15.55	23.62	0.298
S12	TETOUAN	-5.40	35.60	14.74	22.72	1.852
S13	CASABLANCA (ANFA)	-7.67	33.57	14.50	21.94	1.104
S14	ERRACHIDIA	-4.39	31.94	13.19	26.39	0.348
S15	ESSAOUIRA	-9.78	31.52	15.11	20.43	0.882
S16	FES	-4.98	33.93	10.22	24.16	1.329
S17	KASBAT TADLA	-6.28	32.53	12.02	26.88	1.011
S18	MARRAKESH	-8.03	31.62	13.46	27.26	0.609
S19	MEKNES	-5.53	33.88	11.39	23.91	1.335
S20	MIDELT	-4.73	32.68	8.45	21.78	0.479
S21	CASABLANCA (AIRPORT)	-7.58	33.37	11.85	24.01	0.845
S22	OUARZAZATE	-6.90	30.93	12.25	26.99	0.333
S23	OUJDA	-1.93	34.78	10.85	24.31	0.734
S24	RABAT SALE	-6.77	34.05	12.74	22.49	1.390
S25	SAFI	-9.23	32.28	13.83	23.60	1.015
S26	TAZA	-4.00	34.20	12.79	24.62	1.518
S27	DAKHLA	-15.90	23.70	17.12	24.12	0.078

and vertical resolutions, a common location point is created for both observations and models by interpolating the latitude-longitude location points from the observation stations.

The CMIP6 GCMs are forced with Shared Socioeconomic Pathways (SSPs) scenarios to achieve projected values of precipitation and temperature in the future (Raulino et al., 2021). The SSPs are categorized into various groups that represent distinct levels of socio-economic development, such as sustainable development (SSP1-2.6), moderate development (SSP2-4.5), regional competitive development (SSP3-7.0), and fossil fuel-based development (SSP5-8.5) (Almazroui et al., 2020; O'Neill et al., 2013). In this study, the SSP2-4.5 is selected for the evaluation because it assumes that the levels of GreenHouse Gas (GHG) emission will be maintained, while the SSP5-8.5 represents the most pessimistic scenario of the GHG emissions. The SSP2-4.5 is a scenario characterized by moderate socio-economic development and low to moderate GHG emissions, whereas the SSP5-8.5 involves socio-economic factors such as increased inequality and competi-

tion, low economic growth, and high GHG emissions (Meinshausen et al., 2020). The SSP2-4.5 scenario envisions a world in which existing mitigation policies of climate change persist and technological advancements spread moderately facilitating the transition to an economy based on energy efficiency and sources of renewable energy. Conversely, the most pessimistic scenario SSP5-8.5 depicts a world characterized by the intensive use of natural resources and unsuccessful policies in addressing climate change (Riahi et al., 2017). This study aims to clearly ascertain the differences between the two scenarios by examining the cases of mid-level success (SSP2-4.5) and failure (SSP5-8.5) in implementing climate change measures.

3 Methodology and artificial neural networks

Statistical downscaling has received little attention compared to dynamical downscaling. In regions like Morocco, where data are sparse in both time and space, the use of standard statistical methods is argued to be unfeasible, especially that the country is shaped with complex topography. This explains the little use of this class of methods. However, based on the ability of machine learning based methods to tackle complex problems, ANN-based techniques have been demonstrated to alleviate these aforementioned challenges, especially that new data have been recently made available. The procedure adopted in this study is carried out using the following steps:

Step 1. Observed climatic data obtained daily is first converted to monthly averaged values. Using **the bi-linear interpolation method**, the 21 available parameters of the GCMs defining the potential regressors are estimated based on their location and the corresponding geographical coordinates of the gauge station. These parameters are air temperature, relative humidity and geopotential height for five pressure levels (namely, 200, 300, 500, 700 and 850), sea level air pressure, surface air pressure, precipitation and minimum, maximum and mean near-surface temperature parameters.

Step 2. From the 21 **interpolated** potential regressors defined in **Step 1**, only five are retained as input for the ANN model. For each of the observed variables (monthly averaged daily minimum temperature, monthly averaged daily maximum temperature and monthly averaged daily precipitation), the correlation with the regressors is calculated, and the five most correlated variables are retained.

Step 3. An artificial neural network-based model is created, with the input data being the best-correlated five variables of GCMs and the output being the observation data. **These five best-correlated (dominant estimators) vary according to the GCM model, station, or variable to be estimated.**

Step 4. Different performance criteria are used to determine the agreement between the observed and predicted data.

Step 5. **Step 2**, **Step 3**, and **Step 4** are applied to all stations and use all the GCMs of CMIP6. The performance of GCMs to represent climate in the country is determined based on the success order of the models on which they are based.

Step 6. A total of six MME models is obtained using the seven most successful models. **Step 2**, **Step 3**, and **Step 4** are applied to the obtained MMEs, and the results are compared among themselves as well as with the most successful model results. Finally, the model which best represents the region among them is used for the projection.

In this study, the Artificial Neural Networks (ANN) method is used as a Statistical DownScaling Method (SDSM) for GCMs. Notice that the ANN method is frequently preferred by researchers because it can model the relationship between variables without requiring any prior analytical relationships, see (Hosseini Baghanam et al., 2022; Maqsood et al., 2022; Seker and Gumus, 2022) among others. Furthermore, this method has the potential to find the inherent nonlinear relationship between parameters for a complex problem. There exist different architectures for building ANN models, but the feed-forward error back-propagation artificial neural networks (FF-ANN) technique is one of the most widely used architectures (El-Mahdy et al., 2021). Figure 2 illustrates a typical FF-ANN model with n neurons in the input layer (i), m neurons in the hidden layer (j), and one neuron in the output layer (k). Note that the weight terms labeled by w_{ij} and W_{jk} in Figure 2 represent the link between the layers, and they take random values during the model setup. However, they are constantly changing while the comparison between the observed and the predicted values is made during the training process. Finally, the errors propagate backwards as well during which the weights minimize the errors. In the current study, the Levenberg-Marquardt algorithm is used to adjust the weights, see for example (Marquardt, 1963). In this algorithm, the trial-and-error method is used to determine the number of hidden layers. Here, between 1 and 10 hidden layers are used in the prediction model one by one, and the number of the hidden layer with the lowest Root Mean Square Error (RMSE) error is then used in the model. For more details on the ANN we refer the reader to (Rumelhart et al., 1988; Svozil et al., 1997; Sudheer et al., 2002; Keskin and Terzi, 2006) among others.

On the other hand, overfitting is a prevalent issue in machine learning. In this study, the early-stopping approach is employed to address the overfitting problem. Given that this research involves time series data and focuses on future predictions, the dataset is divided into three segments: 60% (1980-2000) for training, 20% (2001-2007) for validation, and the remaining 20% (2007-2014) is used for testing. During the training process, the error for both training and validation datasets are assessed at each iteration. If the error value decreases for both datasets, iterations proceed however, if the RMSE value declines in the training process while increasing in the testing process for six consecutive iterations, the iteration is stopped and the final model is derived.

Table 2: The CMIP6 GCMs for climate projection.

No	Name CMIP6 model	Country	Resolution (° lon ×° lat)	Variant label	Key reference
1	ACCESS-CM2	Australia	1.9° × 1.3°	r1i1p1f1	(Bi et al., 2013)
2	CanESM5	Canada	2.8° × 2.8°	r1i1p1f1	(Swart et al., 2019)
3	CanESM5-CanOE	Canada	2.8° × 2.8°	r1i1p2f1	(Swart et al., 2019)
4	CNRM-CM6-1-HR	France	0.5° × 0.5°	r1i1p1f2	(Voldoire et al., 2019)
5	CNRM-ESM2-1	France	1.4° × 1.4°	r1i1p1f3	(Séférian et al., 2019)
6	EC-Earth3-Veg	Europe	0.7° × 0.7°	r1i1p1f1	
7	FGOALS-g3	China	2.0° × 2.3°	r1i1p1f1	(Li et al., 2020)
8	GFDL-ESM4	USA	1.25° × 1.0°	r1i1p1f1	(Dunne et al., 2020)
9	GISS-E2-1-G	USA	2.5° × 2.0°	r1i1p1f2	(Kelley et al., 2020)
10	INM-CM5-0	Russia	2.0° × 1.5°	r1i1p1f1	(Kulyamin and Volodin, 2018)
11	IPSL-CM6A-LR	France	2.50° × 1.26°	r1i1p1f1	(Boucher et al., 2020)
12	MIROC6	Japan	1.41° × 1.41°	r1i1p1f1	(Tatebe et al., 2019)
13	MPI-ESM1-2-HR	Germany	0.937° × 0.937°	r1i1p1f1	(Gutjahr et al., 2019)
14	MRI-ESM2-0	Japan	1.125° × 1.125°	r1i1p1f1	(Yukimoto et al., 2019)
15	NESM3	China	1.9° × 1.9°	r1i1p1f1	(Cao et al., 2018)

In the present work, five criteria are used to determine the level of agreement between the observed data and the data estimated using GCMs. The criteria used are: Correlation Coefficient (CC), Nash-Sutcliffe efficiency (NSE) (Nash and Sutcliffe, 1970), normalized Root Mean Square Error (nRMSE) (Ahmed et al., 2019), Kling-Gupta Efficiency metric (KGE) (Koch et al., 2018), and Modified Index of agreement (ModIn) (Willmott, 1981) and their corresponding definitions are given by

$$\mathrm{CC} = \frac{\sum_{i=1}^{N}\left(V_p-\overline{V_p}\right)\left(V_o-\overline{V_o}\right)}{\sqrt{\sum_{i=1}^{N}\left(V_p-\overline{V_p}\right)^2}\times\sqrt{\sum_{i=1}^{N}\left(V_o-\overline{V_o}\right)^2}}, \tag{1}$$

$$\mathrm{NSE} = 1-\frac{\sum_{i=1}^{N}\left(V_{p,i}-V_{o,i}\right)^2}{\sum_{i=1}^{N}\left(V_{o,i}-\overline{V_o}\right)^2}, \tag{2}$$

$$\mathrm{nRMSE} = \frac{\sqrt{\frac{1}{N}\sum_{i=1}^{N}\left(V_{p,i}-V_{o,i}\right)^2}}{V_{o(\max)}-V_{o(\min)}}, \tag{3}$$

$$\mathrm{KGE} = 1-\sqrt{(\mathrm{CC}-1)^2+\left(\frac{\overline{V_p}}{\overline{V_o}}-1\right)^2+\left(\frac{\sigma_p/\overline{V_p}}{\sigma_o/\overline{V_o}}-1\right)^2}, \tag{4}$$

$$\mathrm{ModIn} = 1-\frac{\sum_{i=1}^{N}\left|V_{o,i}-V_{p,i}\right|}{\sum_{i=1}^{N}\left(\left|V_{p,i}-\overline{V_o}\right|+\left|V_{o,i}-\overline{V_o}\right|\right)}, \tag{5}$$

where V_o, V_p, $\overline{V_o}$, $\overline{V_p}$ and N represent observed, predicted, mean observed, mean pre-

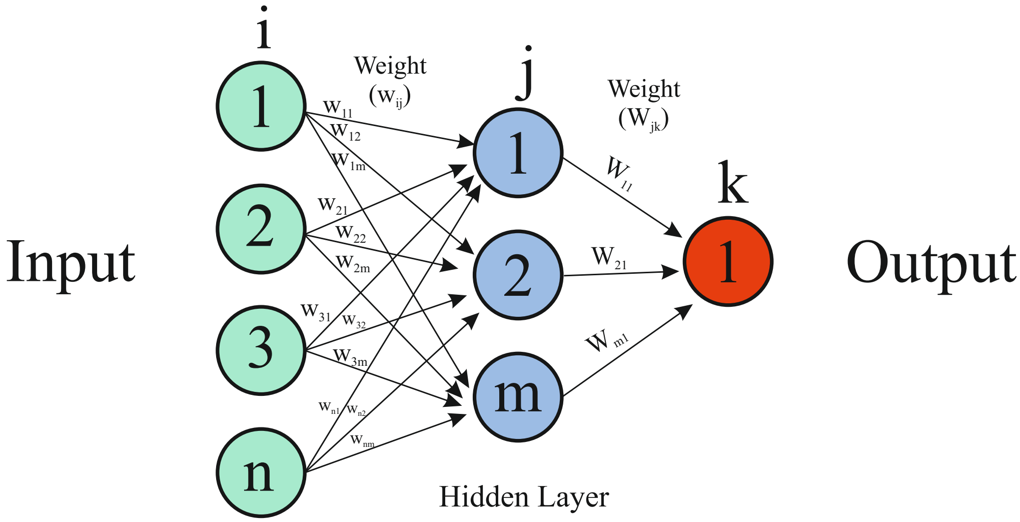

Figure 2: A typical structure of the FF-ANN model.

dicted, and the number of data, respectively. It should be noted that it is challenging to determine with a single criterion whether GCMs are representative or not for climate data in a region because successful GCMs can vary according to any performance criterion used. **This is mainly because each assessment criterion has different limitations. For example, the CC only assesses the linear relationship between two variables and potentially overlooks other forms of relationships. The NSE and nRMSE are sensitive to outliers, the KGE may not accurately measure the model performance when observed data show limited variability, while the ModIn tends to overestimate agreement which may not provide a comprehensive view of the data consistency.** Therefore, the Comprehensive Rating Index (CRI) method (Li et al., 2015), which can evaluate the multiple criteria together, is used to determine the best-represented GCMs for the region under study. Notice that the CRI, frequently used in the evaluation of GCMs (Rivera and Arnould, 2020; You et al., 2018), is calculated as

$$\mathrm{CRI} = 1 - \frac{1}{nm}\sum_{i=1}^{n} Rank_i, \tag{6}$$

where m represents the number of GCMs employed and n represents the number of statistical performance metrics considered. It is worth mentioning that the most successful model is ranked as 1.

4 Results

In this section we present the results obtained from the success of the considered models in representing the region under study. In this section, we first examine the performance of the GCMs and downscaling techniques, then the performance of the multi-ensemble and projection analysis are also assessed.

Table 3: Mean of the performance metrics used in the present study. Here, bold entries represent the most successful model for the relevant metric.

CMIP6 Model	T_{min}					T_{max}					Prep				
	CC	NSE	ModIn	nRMSE	KGE	CC	NSE	ModIn	nRMSE	KGE	CC	NSE	ModIn	nRMSE	KGE
ACCESS-CM2	0.936^{11}	0.865^{11}	0.836^{11}	0.092^{11}	**0.884^{5}**	0.903^{12}	0.806^{12}	0.802^{11}	0.102^{12}	0.833^{7}	**0.457^{5}**	0.192^{8}	**0.502^{5}**	0.164^{8}	0.233^{8}
CanESM5	**0.942^{5}**	**0.875^{5}**	**0.843^{4}**	0.089^{6}	**0.894^{3}**	**0.911^{5}**	0.819^{6}	0.807^{7}	0.099^{8}	**0.845^{3}**	0.423^{15}	0.177^{15}	0.481^{15}	0.165^{12}	0.216^{9}
CanESM5-CanOE	**0.944^{3}**	**0.88^{3}**	**0.845^{3}**	**0.088^{4}**	**0.901^{1}**	**0.914^{2}**	**0.825^{3}**	**0.812^{3}**	**0.098^{5}**	**0.861^{1}**	0.453^{8}	0.184^{12}	**0.513^{1}**	0.165^{14}	**0.237^{4}**
CNRM-CM6-1-HR	0.937^{10}	0.868^{10}	0.838^{10}	0.092^{10}	0.882^{7}	0.904^{11}	0.812^{11}	0.803^{9}	0.102^{11}	0.829^{8}	0.456^{7}	**0.207^{5}**	0.492^{11}	**0.163^{5}**	0.177^{15}
CNRM-ESM2-1	0.938^{9}	0.87^{9}	0.84^{7}	0.091^{9}	0.883^{6}	0.91^{7}	**0.823^{4}**	**0.813^{2}**	**0.097^{4}**	**0.843^{4}**	**0.464^{4}**	**0.216^{2}**	**0.506^{4}**	**0.162^{1}**	**0.235^{5}**
EC-Earth3-Veg	**0.947^{1}**	**0.888^{1}**	**0.852^{1}**	**0.084^{1}**	**0.896^{2}**	**0.919^{1}**	**0.837^{1}**	**0.819^{1}**	**0.093^{1}**	**0.847^{2}**	0.443^{11}	0.178^{14}	0.498^{8}	0.166^{15}	0.203^{13}
FGOALS-g3	0.935^{12}	0.86^{12}	0.834^{12}	0.094^{12}	0.864^{14}	0.91^{6}	0.818^{7}	0.805^{8}	0.1^{10}	0.829^{10}	0.45^{10}	0.195^{7}	0.494^{9}	0.164^{7}	0.205^{12}
GFDL-ESM4	0.941^{6}	0.874^{7}	0.839^{9}	0.09^{8}	0.866^{13}	0.91^{8}	0.816^{9}	0.803^{10}	0.1^{9}	0.815^{13}	0.438^{13}	0.182^{13}	0.5^{7}	0.165^{9}	0.206^{11}
GISS-E2-1-G	0.927^{14}	0.852^{14}	0.826^{14}	0.098^{14}	0.877^{10}	0.898^{14}	0.8^{14}	0.794^{14}	0.106^{14}	0.827^{11}	0.45^{9}	0.184^{11}	0.491^{13}	0.165^{11}	**0.239^{3}**
INM-CM5-0	0.94^{8}	0.872^{8}	0.84^{8}	0.09^{7}	0.875^{12}	0.91^{10}	0.813^{10}	0.799^{12}	0.099^{7}	0.814^{14}	0.432^{14}	0.195^{6}	0.491^{12}	0.163^{6}	0.212^{10}
IPSL-CM6A-LR	0.931^{13}	0.858^{13}	0.834^{13}	0.094^{13}	0.88^{8}	0.901^{13}	0.803^{13}	0.796^{13}	0.103^{13}	0.829^{9}	**0.472^{2}**	**0.209^{4}**	**0.507^{2}**	**0.163^{4}**	**0.252^{1}**
MIROC6	0.941^{7}	0.874^{6}	0.841^{6}	**0.088^{5}**	0.877^{9}	**0.913^{4}**	**0.826^{2}**	0.807^{6}	**0.097^{2}**	**0.837^{5}**	**0.469^{3}**	**0.212^{3}**	**0.506^{3}**	**0.162^{3}**	0.235^{6}
MPI-ESM1-2-HR	**0.944^{4}**	**0.878^{4}**	**0.842^{5}**	**0.086^{3}**	0.875^{11}	0.91^{9}	0.817^{8}	**0.808^{5}**	0.098^{6}	0.821^{12}	0.442^{12}	0.185^{10}	0.494^{10}	0.165^{10}	0.235^{7}
MRI-ESM2-0	0.926^{15}	0.847^{15}	0.823^{15}	0.098^{15}	0.861^{15}	0.895^{15}	0.792^{15}	0.789^{15}	0.108^{15}	0.802^{15}	0.457^{6}	0.186^{9}	0.489^{14}	0.165^{13}	0.193^{14}
NESM3	**0.946^{2}**	**0.885^{2}**	**0.85^{2}**	**0.085^{2}**	**0.887^{4}**	**0.913^{3}**	**0.823^{5}**	**0.811^{4}**	**0.097^{3}**	0.836^{6}	**0.483^{1}**	**0.219^{1}**	0.502^{6}	**0.162^{2}**	**0.25^{2}**

4.1 Performance of GCMs and Downscalling method

We first investigate the ability of the proposed downscaling approach using different CMIP6 models to accurately represent the historical data in Morocco for all the considered stations. The metrics defined in the previous section are used to evaluate the performance of the ANN-reduced model in predicting the observation data. Violin plots of the calculated metric values for each CMIP6 model are shown in Figure 3 for T_{min}, T_{max} and Prep. Here, the width of the curve in the violin plots indicates that the calculated metric value is concentrated in that region, and the boxes inside the violins represent the region with values between **the first quartile (Q1) corresponding to the value below which 25% of the data points lie, and the third quartile (Q3) indicating the value below which 75% of the data points.** The results demonstrate that two models, namely EC-Earth3-Veg and NESM3, successfully represented the behavior of T_{min}. This is confirmed by the values of the different evaluation metrics considered here, except for NESM3 where the value of KGE does not translate a good fit of the model to the observation. In the violin plots of T_{max} shown in Figure 3, it is seen that differences between the models are not very high, and a general agreement between the models and the observation data is observed except for ACCESS-CM2, GISS-E2-1-G and IPSL-CM6A-LR. In addition, it can be concluded that EC-Earth3-Veg and CanESM5-CanOE models show a similar prediction performance for almost all considered stations. However, a simple inspection of violin plots of the precipitation values depicted in Figure 3, it can be concluded that, unlike the temperature values, the distribution is not similar and there are significant differences between these models. For example, although some models (such as GFDL-ESM4 and CanESM5) give a CC value very close to 0, the NESM3 model differs from others in terms of CC and NSE, and EC-Earth3-Veg distinguishes from other models according to the ModIn metric.

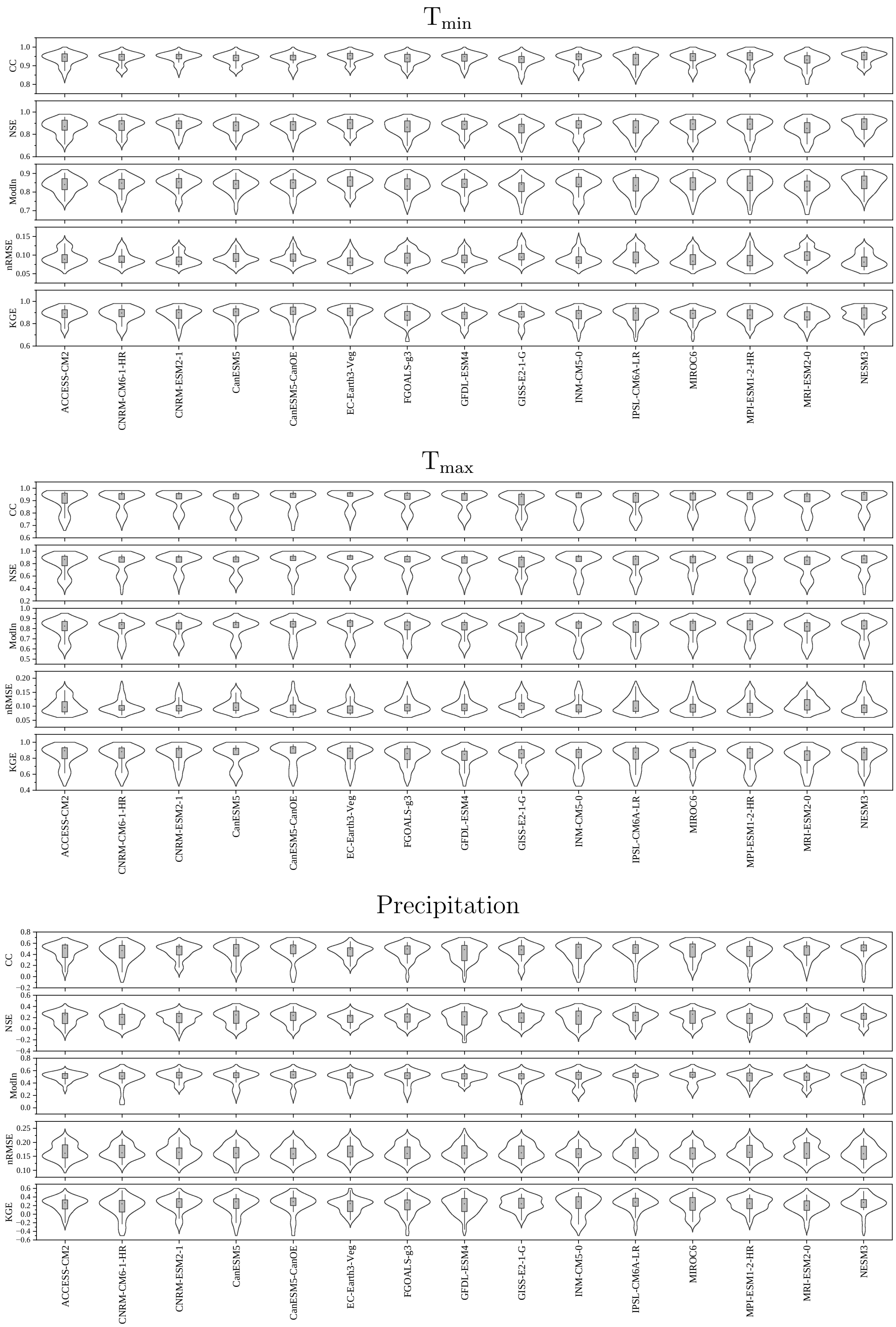

Figure 3: Violin plots of the considered performance criteria for estimating T_{min} (top plot) and T_{max} (middle plot) and precipitation (bottom plot).

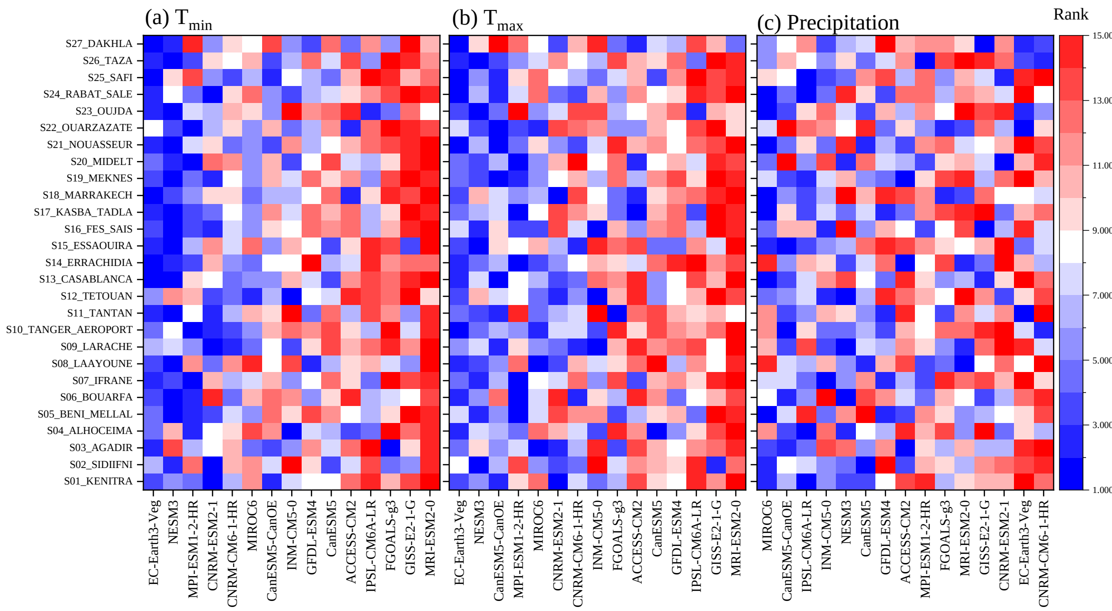

Figure 4: Station-based heat map of the CRI values for GCMs obtained for T_{min} (left plot), T_{max} (middle plot) and Prep (right plot).

In addition to the violin plots, the averaged metric values obtained at all stations are calculated for each parameter and for all the considered CMIP6 models and are presented in Table 3. Notice that the numbers given as superscripts in this table indicate the model's rank in the metric, and the most successful models are shown in bold. For the temperature T_{min}, the averaged CC value of the predicted and measured values is between 0.925 and 0.947. These results, which are quite close to each other, are similar to other metrics, compare results in Table 3. Indeed, when metrics of the temperature T_{max} are analyzed, it is determined that the agreement is lower than the temperature T_{min}, and the averaged CC value is between 0.894 and 0.919. For values of the precipitation, it is determined that the averaged CC value is 0.482 in the best model, where the fit is lower than for the temperature values. Note that these values are averaged values, and it should be considered that low or high values at a station may affect the averaged values.

Although the general success displayed by the proposed models, it is seen that the obtained results vary depending on the considered metric. Therefore, since each method metric's calculation and approach are different, the accuracy of the prediction should be understood from the perspective of the corresponding metric. For example, the CC metric determines the compatibility of two data sets, while the nRMSE metric calculates the difference between the predicted and observation values. The CRI metric evaluates the performance of a model's prediction and determines the most successful model according to all metrics. The success ranks of models used in the 27 stations are determined according to the calculated CRI values and illustrated in Figure 4. In this figure, models with the minimum averaged CRI values (i.e. the most successful models) are ranked from left to right to understand the distribution of the mean CRI values.

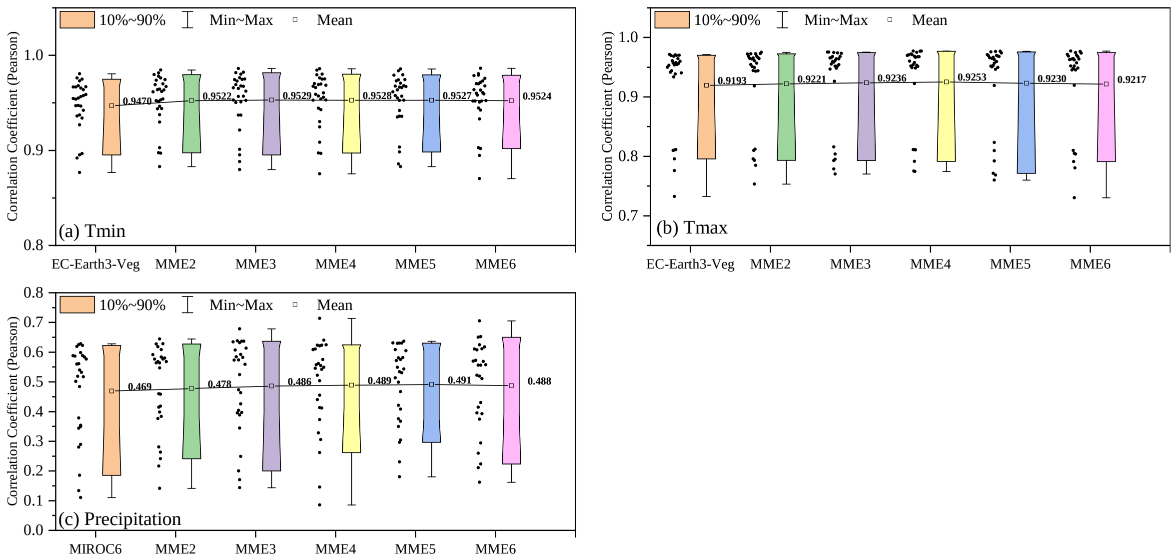

Figure 5: Determination of the best MME for T_{min} (a), T_{max} (b) and Prep (c).

Regarding the estimation of temperature T_{min}, the EC-Earth3-Veg, NESM3, MPI-ESM1-2-HR, CNRM-ESM2-1 and CNRM-CM6-1-HR are roughly the models that have the most successful rate. It is also evident that simulations of the EC-Earth3-Veg and NESM3 are robust as they are the most successful models in almost all stations for the temperature T_{min}. Similarly these two models are also robust for the estimation of the temperature T_{max} followed by CanESM5-CanOE, MPI-ESM1-2-HR and MIROC6, respectively. For the precipitation, as it can be seen from Figure 4, there is not a single model that can be robust for most of the stations. However, the MIROC6, CanESM5-CanOE, IPSL-CM6A-LR, INM-CM5-0 and NESM3 have high success rates.

4.2 Performance of multi-model ensemble

Although the best models based on the CRI parameter have been found to be satisfactory in a significant part of the considered stations, especially for the temperature variables, some stations are not well represented. In particular, the prediction of precipitation is not accurate for all considered stations. Therefore, a Multi-Model Ensemble (MME) that better represents the entire region is created in the current study. For this purpose, the MMEs are obtained by averaging the most successful models following their ranks. For sake of simplicity, MMEk is used to denote a MME obtained using the best k successful models based on the CRI criteria. For example, the MME2 is derived from the mean of the two most successful models according to the CRI values whereas, the MME4 is obtained using the most successful top four models. In this manner, a total of five different MMEs are obtained using the top six most successful models. Using these MMEs as input, **Step 2**, **Step 3** and **Step 4** described in Section 3 are applied. Hence, the results obtained from the calculations for T_{min}, T_{max} and Prep are compared between themselves as well as with the most successful model. In this

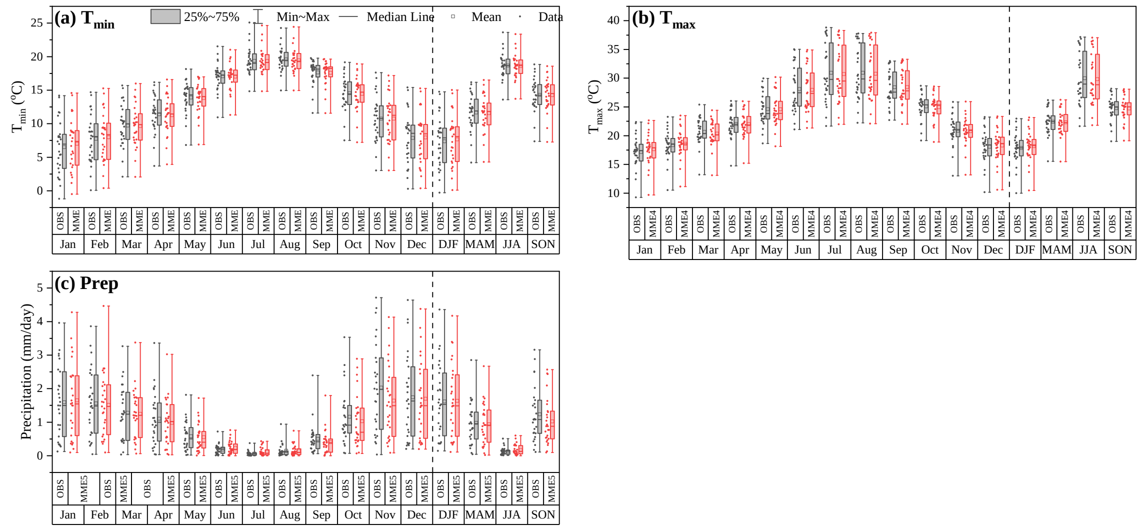

Figure 6: Distribution of the best MME and observed values for monthly and seasonal time scales for T_{min} (a), T_{max} (b) and Prep (c).

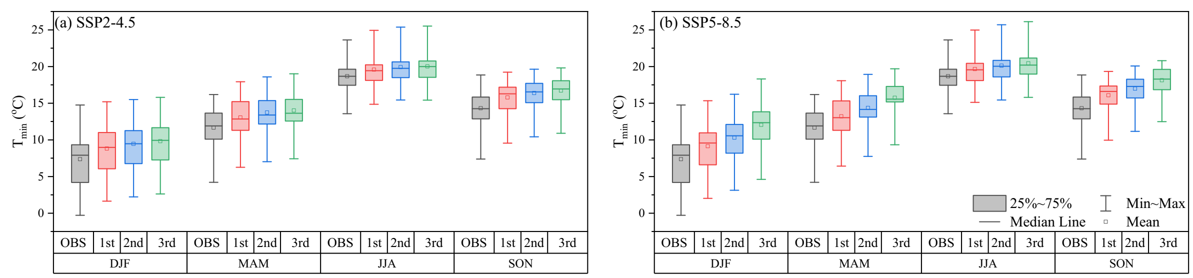

Figure 7: **Observed measurements and future projections** of the seasonal T_{min} for SSP2-4.5 (a) and SSP5-8.5 (b).

comparison, determining the number of models to be used in the MME is a challenging task. For this reason, the mean CC, which is also preferred by different researchers (Iqbal et al., 2020; Seker and Gumus, 2022), is considered in the assessment of MME. In this approach, the CC values between the model results and the observation data are calculated for each station, and how each new model added for the MME affects the prediction performance is evaluated by considering the averaged CC for all stations. The results of this approach for T_{min}, T_{max} and Prep are also included in Figure 5.

It is evident that the MMEs created according to the averaged CC values in all climate parameters perform better than the most successful model. For the temperature T_{min}, the MMEs created using the MME3 do not increase the performance but slightly decrease it, and for the temperature T_{max}, the performance of the model decreases when using the MME4. On the other hand, for precipitation values, it is observed that the model performance improves until the MME5, and the performance decreases after adding the next model. Therefore, the MME3 (EC-Earth3-Veg, NESM3 and MPI-ESM1-2-HR) is used for T_{min}, MME4 (EC-Earth3-Veg, NESM3, CanESM5-CanOE and MPI-ESM1-2-HR) for T_{max} and MME5 (MIROC6, CanESM5-CanOE, IPSL-CM6A-

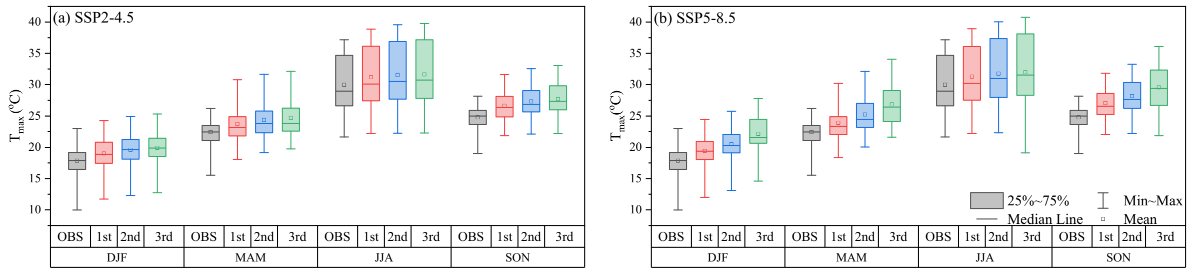

Figure 8: **Observed measurements and future projections** of the seasonal T_{max} for SSP2-4.5 (a) and SSP5-8.5 (b).

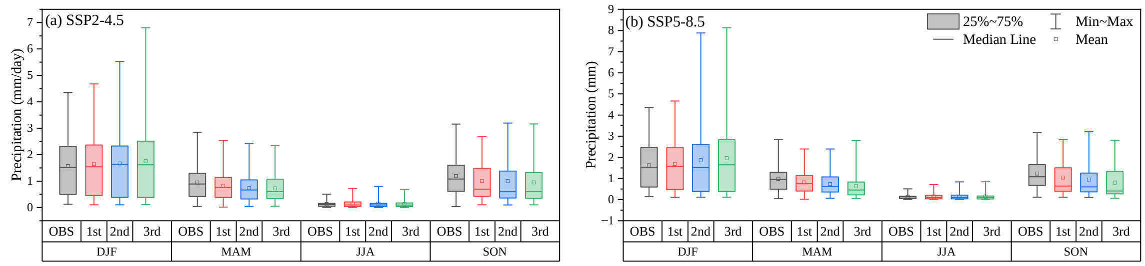

Figure 9: **Observed measurements and future projections** of the seasonal Prec for SSP2-4.5 (a) and SSP5-8.5 (b).

LR, INM-CM5-0 and NESM3) for Prep.

The box plot graphs shown in Figure 6 are presented to demonstrate the agreement between the measured values for T_{min}, T_{max} and precipitation, and the most successful MME. These plots present the mean, median, minimum, and maximum values, along with the values ranges of Q1 and Q3. These graphs reveal that the MMEs for T_{min} and T_{max} are quite successful in predicting historical data. Additionally, it can be clearly seen that the values obtained with MME for T_{min} and T_{max} in March, April and May are slightly lower than the observed values, while the prediction performance is better in other months. Concerning the precipitation values, although the agreement is not as successful as in temperature values, there are no excessive differences between the values. Except for the summer months, the precipitation values calculated using the MME are underestimated, with the highest differences occurring in September, October and November. However, it can still be confirmed that the performance of predicting monthly and seasonal precipitations is satisfactory.

4.3 Projection analysis

In this section, the possible future changes in the temperature T_{min}, T_{max}, and precipitation for Morocco are analyzed using the generated simulations with the developed MMEs. Firstly, the temporal variations of these variables are analyzed for both seasonal and annual time scales, then the spatial variations are evaluated. The evaluation period considered in the present work is 2025-2100 and it is split into three separate ranges. Consequently, changes are analyzed for the following periods: 2025-2049, 2050-2074,

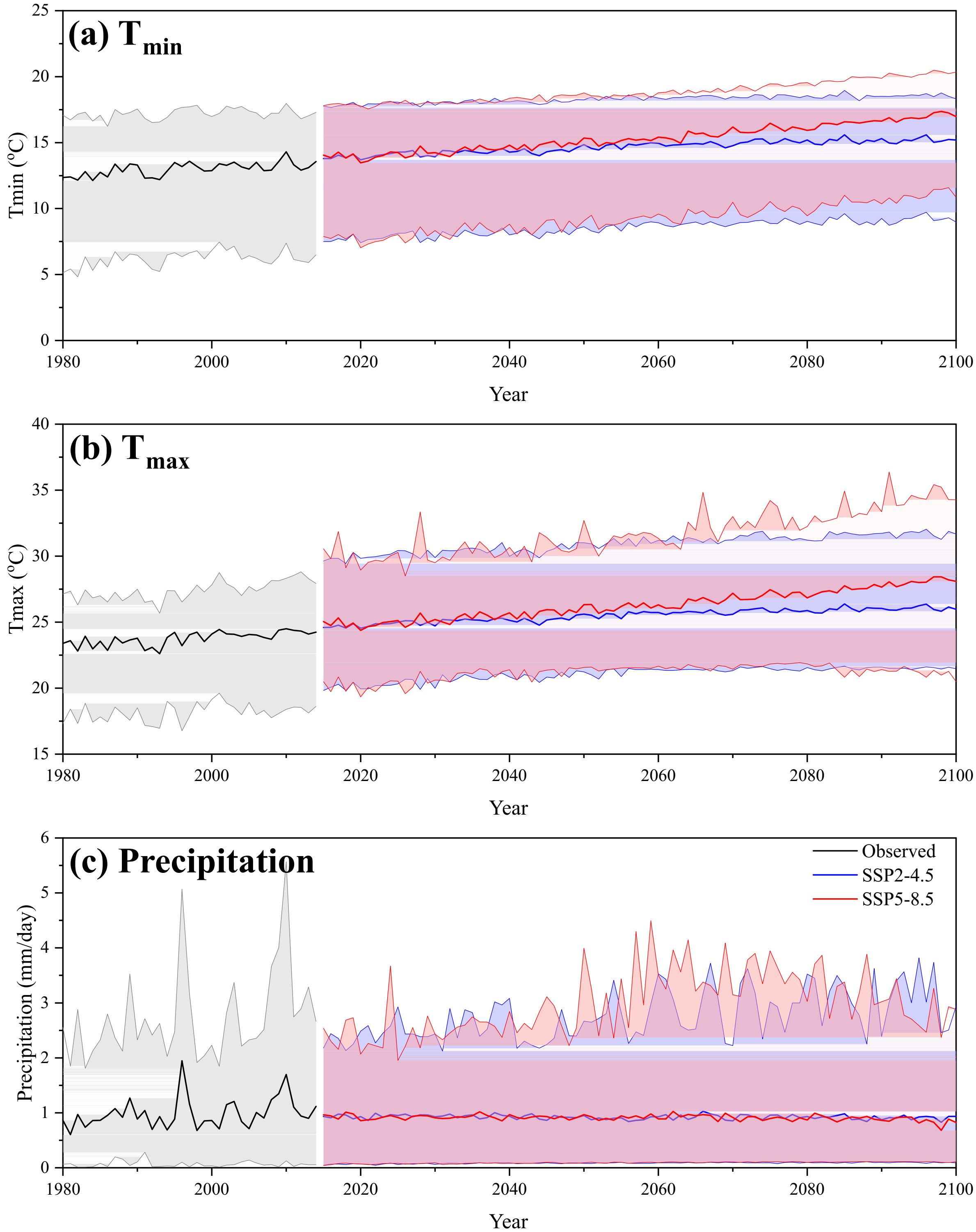

Figure 10: Changes in the observed (1980–2014) and two future projections (2015-2100) for T_{min} (a), T_{max} (b) and Prep (c).

and 2070-2100, which are referred to as the near future (NF), mid future (MF), and far future (FF), respectively. The future projections under the SSP2-4.5 and SSP5-8.5

scenarios for $T_{\min}$ are shown in Figure 7 for each season. An important increase of daily minimum temperature is expected under both scenarios and during all seasons for the three periods. The most important increase will occur during the NF periods, while in the MF and FF, the temperature T_{min} will remain roughly at the same values as those displayed during NF. Concerning the seasonal changes, the main increasing will occur during winter (by 19%, 9% and 5% in NF, MF and FF respectively) where the increase could reach approximately 1.5° following the SSP2-4.5 scenario and 1.8° following the SSP5-8.5 scenario. The increase of temperature is also expected during the other seasons with an increase of 1.5° during the spring and of 1° during the fall. It should also be noted that, while the major part of the expected change will generally occur in NF, the winter averaged daily minimum temperature will be subject to an important increase following the SSP5-8.5 scenario during the whole century. Needless to mention that the increase rate may reach 60% compared to historical records in FF, which will lead to an addition of 4.6° to the actual daily minimum temperature.

The results obtained for the seasonal projection in the temperature $T_{\max}$ according to the SSP2-4.5 and SSP5-8.5 scenarios are shown in Figure 8. It is clear that increases in values of $T_{\max}$ for the SSP2-4.5 are found to be 1.8 °C (7%), 0.7 °C (3%), and 0.4 °C (1%) for NF, MF, and FF, respectively. Moreover, changes in DJF and MAM are observed to be very close in percentage and magnitude, these increases are calculated to be approximately 2 °C (10%) in total. On the other hand, similar to $T_{\min}$, the increase in $T_{\max}$ for the JJA season is relatively low, both in terms of the value and percentage, and increases for NF, MF, and FF in the JJA are found to be 1.2 °C, 0.4 °C, and 0.1 °C, respectively. Except for the JJA season, the amount of increase in FF for the SSP5-8.5 scenario increases in comparison to the previous time period, similar to $T_{\min}$. For example, while the increase in NF is 1.5 °C (8.4%) for DJF, becomes 1.7 °C (9.5%) in FF, and for MAM, the increase in NF is 1.5 °C (6.7%), and it reached 1.6 °C (7.2%) in FF. In addition, although the percentage increase in values of $T_{\max}$ is less than that in values of $T_{\min}$, it is understood that they are also likely to exhibit a significant change when considered on a value basis. In particular, the amount of increase predicted as 2.9 °C (10%) in total for the SSP2-4.5 scenario in the SON season reaches 4.9 °C for the SSP5-8.5 scenario.

Figure 9 presents results for the seasonal projection of the precipitation according to the SSP2-4.5 and SSP5-8.5 scenarios. It should be noted that the rate of change in the precipitation is different than that in the temperature. An important intra-seasonal variability is expected following the SSP2-4.5 scenario. For example, while DJF is increasing (a total of 12%), MAM is decreasing (a total of 24%). In the SON season, there is a significant decrease in NF (about 15.8%) whereas, in the following years this rate of decrease becomes moderate (about -0.6% in MF and about -4.1% in FF). Although there is an increase in NF and a decrease in MF and FF in the summer months, these changes might not be considered as significant because the precipitation values during this season are low. In the SSP5-8.5 scenario, it can be concluded that the averaged precipitation shows relatively clearer changes. For example, while the rate of increase in DJF is 12% in the SSP2-4.5 scenario, it is 21% in the SSP5-8.5 scenario,

Table 4: Linear trends of observed and projected variables.

Period	**T_{min} (°C/decade)**		**T_{max} (°C/decade)**		**Prep (mm/day/decade)**	
OBS (1980-2014)	0.299		0.337		0.082	
	SSP2-4.5	**SSP5-8.5**	**SSP2-4.5**	**SSP5-8.5**	**SSP2-4.5**	**SSP5-8.5**
NF (2025-2049)	0.093	0.36	0.114	0.365	-0.019	-0.003
MF (2050-2074)	0.164	0.388	0.175	0.392	0.016	-0.003
FF (2075-2100)	0.073	0.47	0.112	0.525	-0.014	-0.034
ALL (2025-2100)	0.16	0.41	0.164	0.439	-0.004	-0.009

and the decrease in MAM is calculated as 35.3% from 23.7% in the SSP2-4.5 scenario. Although there is an increase in the rate of decrease in SON, the change is not as high as in DJF and MAM.

In order to examine changes in the future temperature and precipitation patterns of the country according to different scenarios, the changes are investigated over the annual averaged values and are displayed in Figure 10 for T_{min}, T_{max}, and precipitation. Here, the black line in the plots represents the average of all observed stations, the blue and red lines represent the possible changes according to the SSP2-4.5 and SSP5-8.5 scenarios, and the filling in of the same colour indicates the range of the lowest and highest values at the stations. For the temperature T_{min} and T_{max}, it is clear that the values calculated according to the SSP2-4.5 and SSP5-8.5 scenarios for the year 2040 are quite close to each other, but later the temperature values calculated with the SSP5-8.5 scenario diverge since they are higher. On the other hand, it is evident that there are no significant differences between the trends of the two scenarios considered for precipitation which are quite similar. It is worth mentioning that another major important feature of these results remains the range of uncertainty which translates the spatial variability already observed in historical records. This may further increase under the impact of climate change which shall be discussed later in the present study.

On the other hand, since only a general change structure can be seen from these plots, in order to make a more detailed evaluation, the linear slopes for OBS, NF, MF, and FF are calculated and listed in Table 4. According to the results from this table, the historical linear trend slope for T_{min} is calculated as 0.299 °C per decade. For the SSP2-4.5 scenario, it is 0.093, 0.164, and 0.073 °C/decade for NF, MF, and FF, respectively, and 0.16 °C/decade for 2025-2100. Furthermore, linear trend slopes calculated with the SSP5-8.5 are 0.36, 0.388, 0.470, and 0.410 °C/decade for NF, MF, FF, and all time scales, respectively. Thus, when the trend slopes are considered, it is clearly understood that the slope values will decrease according to the SSP2-4.5

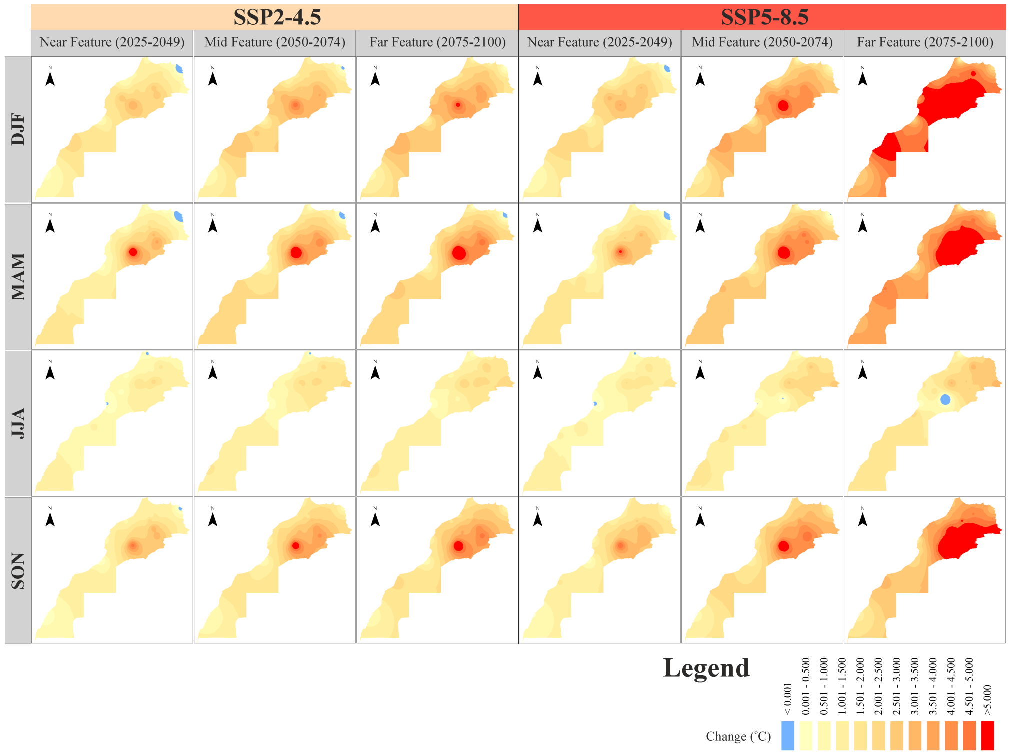

Figure 11: Spatial distribution of future changes in T_{min} according to MME for seasons.

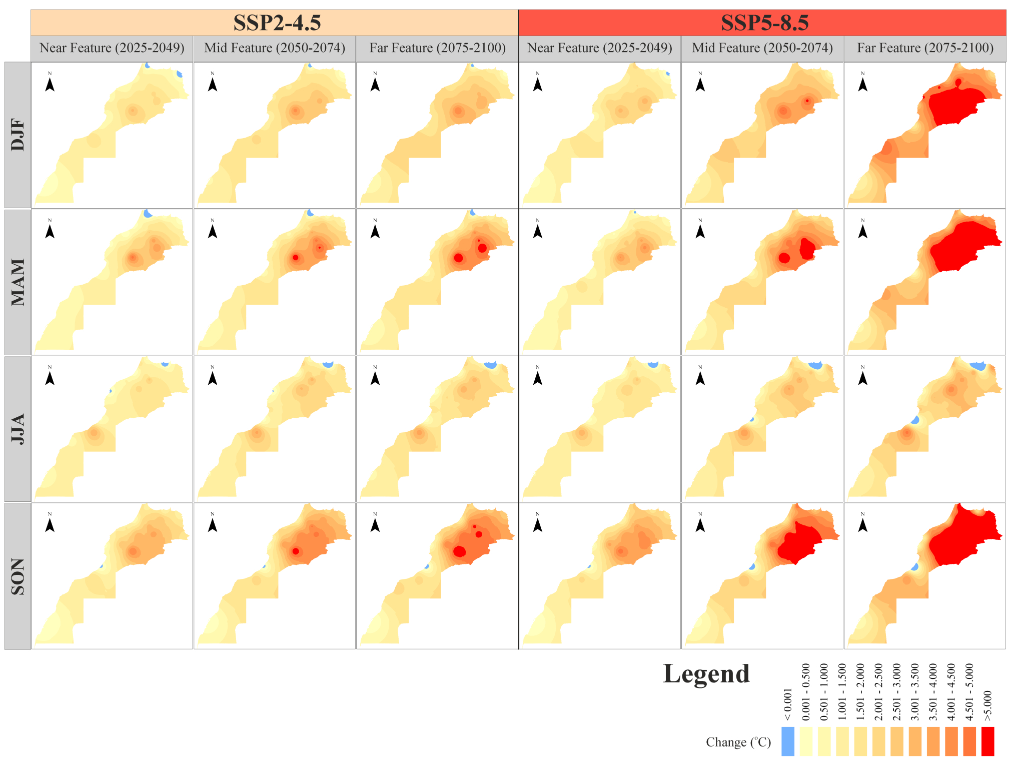

Figure 12: Spatial distribution of future changes in T_{max} according to MME for seasons.

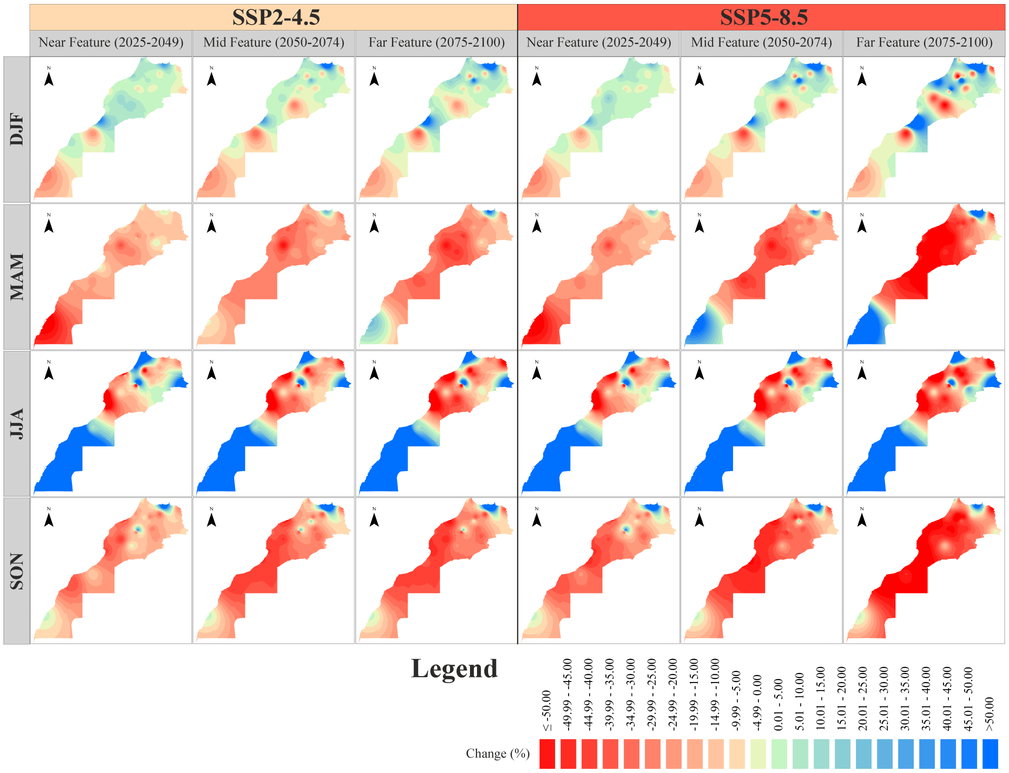

Figure 13: Spatial distribution of future changes in Prep according to MME for seasons.

scenario and will increase according to the SSP5-8.5 scenario using the annual averaged values. A similar situation also occurred in T_{max} for which, the slopes of the linear trend calculated in all periods according to the SSP2-4.5 scenario are lower than the slope of the observation values. In addition, while the linear trend slope of the observed values in Prep is 0.082 mm/day/decade, it turned negative in the SSP2-4.5 and SSP5-8.5 scenarios, and the amount of decrease is higher in the SSP5-8.5 scenario.

As suggested above, in addition to the temporal changes, substantial spatial variability is also expected under climate change impact. For this purpose, the spatial variability of seasonal and annual changes are also analyzed in this section. The spatial distribution of T_{min}, T_{max}, and precipitation for two different scenarios and four seasons are displayed in Figure 11, Figure 12, and Figure 13, respectively. The changes in these plots indicate the difference between the mean of 1980-2014, the reference period, and the percentage change in the precipitation. A simple analysis of changes in T_{min} values shown in Figure 11 according to the SSP2-4.5 scenario reveals that temperatures will continuously increase as the time period rises in the DJF, MAM, and SON seasons *i.e.*, in the period from NF to FF. More precisely, according to the SSP2-4.5 scenario, it is predicted that a serious temperature increase will occur in the eastern part of the country in the MAM season, even in the NF. Since this increase would also occur in MF and FF in DJF and SON in the same region, it should be noted that the relevant region would face a serious temperature increase even in a relatively optimistic scenario. In the SSP5-8.5 scenario for T_{min}, the situation is even more remarkable during the DJF,

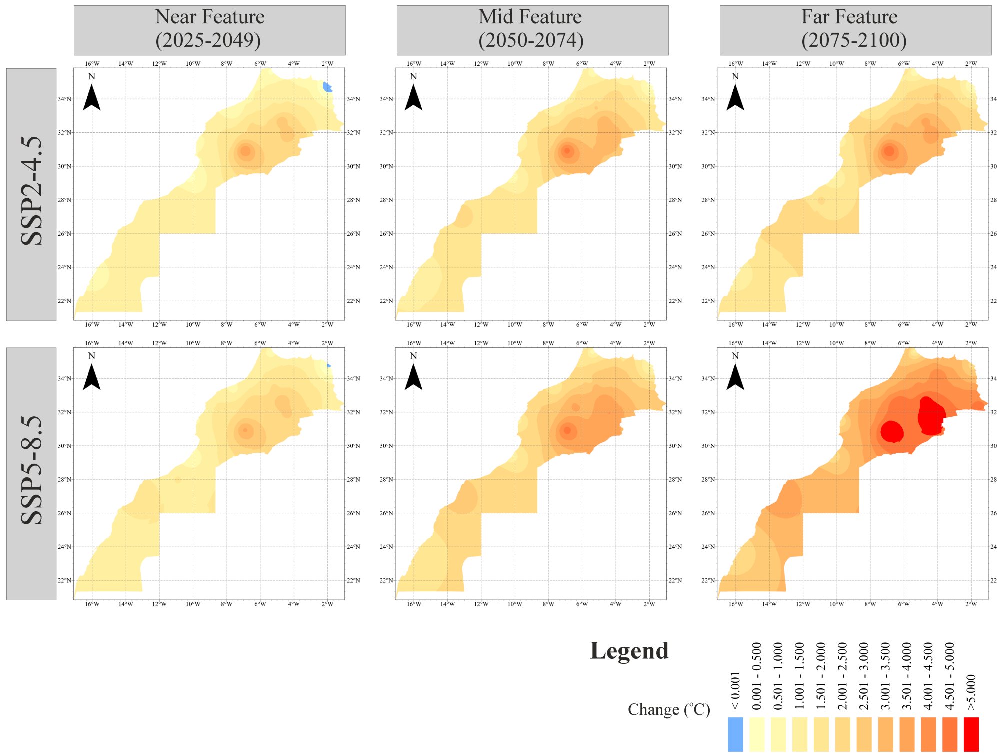

Figure 14: Spatial distributions of future change in T_{min} according to MME.

MAM, and SON seasons. For example, in the SSP2-4.5 scenario, regions where the temperature increases above 5 ° C will occur are limited while, in the FF period of the SSP5-8.5 scenario, this increase would occur in almost half of the country in DJF. In contrast to these increases in DJF, MAM, and SON in Morocco, it is observed that the increase of temperature in the JJA season for both scenarios is limited compared to other seasons, even in the FF time period of the SSP5-8.5 scenario, there is an increase in a small region in the central part of the country. It is also noteworthy that increases in the southern part of the country are generally lower than the rest.

The spatial distributions of possible changes for the temperature T_{max} parameter according to seasons and two different scenarios are depicted in Figure 12. Although the general structure of T_{max} is similar to those obtained for T_{min}, the increase in T_{max} is higher than expected. The increases in T_{max} values in JJA are also limited compared to other seasons. However, one should note that this value is already high during the present climate. Moreover, according to the SSP5-8.5 scenario, a significant part of the northern part of the country would face an increase of more than 5 ° C in FF. Figure 13 presents the spatial distribution of the possible changes in precipitation according to seasons and two different scenarios. In the SSP2-4.5 scenario, the largest difference in the rate of change in DJF occurred in NF, and it is understood that there is not much change in the following periods. According to this scenario, precipitation generally increases in the north while it decreases in the south region. Although a similar situation is observed for the SSP5-8.5 scenario, it is recognized that changes in the precipitation are more pronounced as the time period progresses in this scenario.

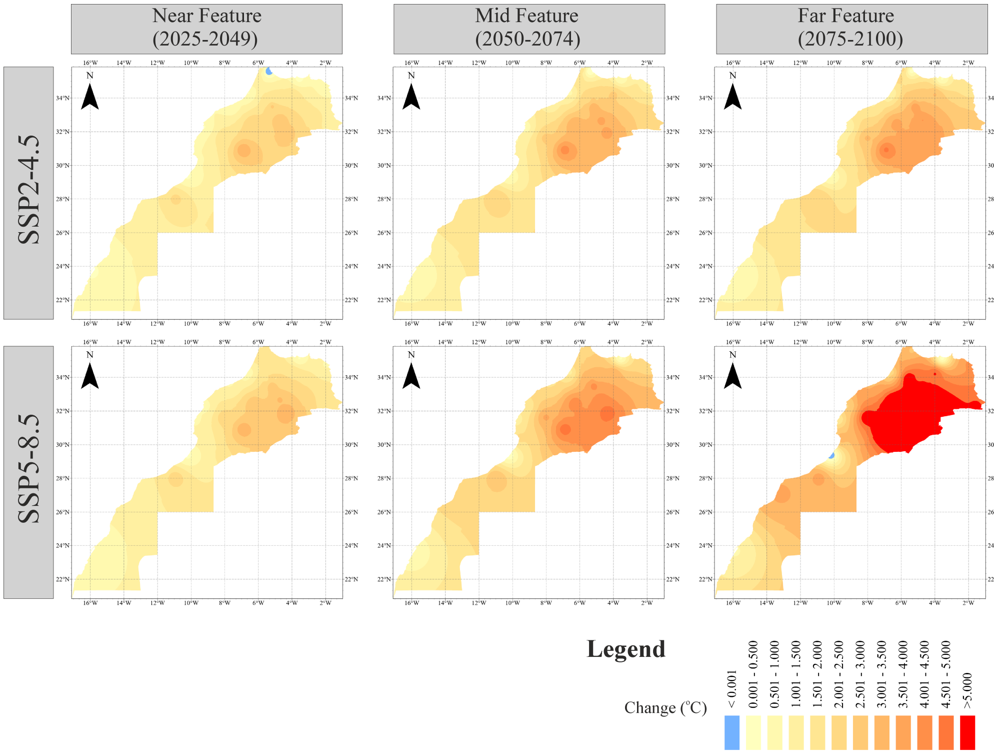

Figure 15: Spatial distributions of future change in T_{max} according to MME.

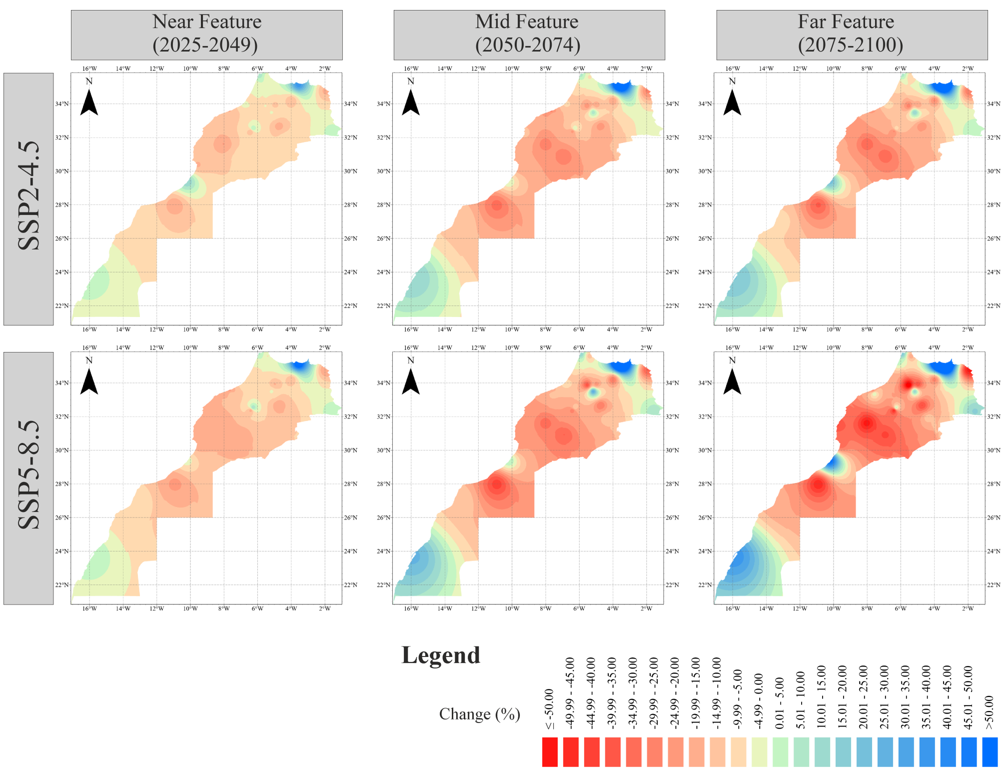

Figure 16: Spatial distributions of future change in precipitation according to MME.

The MAM and SON seasons give similar results. In these seasons, according to both scenarios, it is revealed that the precipitation would decrease significantly in a vast part of the country. Under the SSP5-8.5 scenario, the precipitation during the spring could increase in the Sahara region. In the JJA, although there is an increase in the southern part of the country and a decrease in the northern part, it is considered that these increases or decreases are not very significant since the precipitation in this season is generally low.

Spatial distributions of annual averaged values are given in Figure 14, Figure 15, and Figure 16 for the temperature T_{min}, T_{max}, and the precipitation, respectively. It is clear that T_{min} and T_{max} exhibit similar features in annual values as in seasonal values, and the amount of increase in temperatures rises as periods advance, according to the SSP2-4.5 and SSP5-8.5 scenarios. In addition, it is remarkable that in the SSP5-8.5 scenario, the increase in FF reaches the highest level, and more than 5° C is projected in the northern region. The annual changes in the precipitation values show that there would be a significant decrease in the precipitation in the country except for the Sahara region. It is also clear from Figure 18 that an increase in the precipitation is likely to occur in a small region of the northern region. The decrease may reach up to 30% in FF according to the SSP2-4.5 scenario and it exceeds 50% in the SSP5-8.5 scenario at the same period. Although this decrease in the precipitation would be limited in NF, it is predicted that the increase would reach the highest levels in FF.

5 Discussions

In the present study, projections of monthly averaged daily total precipitation, monthly averaged maximum and minimum temperatures with 15 GCMs available under CMIP6 for Morocco, an important region of north-west Africa, are carried out using an ANN-based statistical downscaling method. The data are analyzed as historical (1980-2021), near future (2025-2049), mid future (2050-2074) and far future (2075-2100). The best three GCMs for simulating historical precipitation are MIROC6, CanESM5-CanOE and IPSL-CM6A-LR, respectively. The two best GCMs for simulating T_{max} and T_{min} are EC-Eart3-Veg and NESM3. The MPI-ESM1-2-HR GCM is the third-best GCM for T_{min}, and the CanESM5-CanOE is the third-best model for the temperature T_{max}. It should be stressed that in addition to the current work, the EC-Eart3-Veg model, which was found to be a successful model in a study conducted by (Dey et al., 2022) in India, was also found to show excellent skills in studies conducted by (Babaousmail et al., 2021) in the north Africa region, (Nashwan and Shahid, 2022) in Egypt, and (Majdi et al., 2022) in the MENAP (Middle East, North Africa, Afghanistan, Pakistan, and Turkey) region.

The performance of the GCMs to simulate historical precipitation, maximum, and minimum temperatures are evaluated individually, and it is found that the capability of these models vary from a station to another and the parameter estimated namely, the temperature T_{min}, T_{max} and the precipitation. It is also clear that while the top two GCMs (*i.e.* EC-Eart3-Veg, NESM3) are the same for maximum and minimum temperatures, the accuracy of other models vary considerably. In addition, the EC-Eart3-Veg model, which has a good performance in simulating maximum and minimum temperatures, does not perform well in simulating the precipitation. Here, the MIROC6 model, which performs better than the other models to predict the precipitation, does not perform well in simulating the maximum and minimum temperatures as opposed to the other aforementioned models. In many other studies in the literature, it has been emphasized that biases and uncertainties in the GCMs limit the performance of their simulations for different regions (Wu et al., 2015; Xu et al., 2019; Abbas et al., 2022). Therefore, it is essential to make multi-model ensemble projections instead of climate projections based on single-model projections. Previous studies conducted by Dey et al. (2022); Seker and Gumus (2022); Iqbal et al. (2020); Guo et al. (2021); Nashwan and Shahid (2022) have shown that uncertainties can be reduced through MMEs created using GCMs with the best representation capability. It has also been found that the performance of simulations using the MME created for the present study supports the previous studies such that the MMEs are more successful than the single model for simulating historical climate variables.

The analysis of climate change impact on the temperature T_{min} reveals that an important amount of increase is to be expected in the future, following both SSP2-4.5 and SSP5-8.5 scenarios. The major part of the increase will occur in the near future according to both scenarios. Moreover, the northern part of the country is more likely to experience substantial increase. These results are in good agreement with those presented by (Hamed et al., 2022) in the MENA region, with some differences on the rate of increase in the southern region. Furthermore, (Carvalho et al., 2021) found similar results for the potential changes in the temperature T_{min} in the region, with some differences in the seasonal variability where the study concluded that the important changes will occur during the winter and summer as opposed to the present study which reveals that the major increases will be observed during the winter and fall time.

On the other hand, projections for the temperature T_{max} in the study area are found to be consistent with the temporal changes in the temperature T_{min}. However for the considered conditions, the temperature T_{max} increases more than the temperature T_{min}. In addition, although the spatial changes are similar to those displayed by the spatial distribution of T_{min}, the increase is wider from a spatial point of view. In this regard, especially in the autumn months, increases of up to 5 ° C in T_{max} for the SSP5-8.5 scenario are to come to the forefront. Seasonal changes demonstrated in the current study, are consistent with those reported in the study by (Lachgar et al., 2021), although the increasing amount is different. In addition, increases in values of the temperature T_{max} are more pronounced, especially in areas within high-altitude regions in the north and northeast parts of the country.

The change in the precipitation exhibits a different structure compared to the temperature. Here, a projected decrease, regarding the precipitation of 30% following the SSP2-4.5 scenario and of 50% following the SSP5-8.5 scenario are expected. Besides, based on the presented results, an increase of precipitation during winter time (DJF) is observed for the three considered future periods. This is considered as a surprising result, with respect to the literature. In fact, many previous studies have highlighted that a decrease of precipitation is expected for all seasons in the future scenarios. For example, Tuel et al. (2021) used a CMIP5 multi-model to force a high-resolution regional climate model over the west part of the Mediterranean region. This study shows that a consistent decrease of precipitation is expected during winter time using the three GCMs. Those results were later confirmed with CMIP6 simulations in (Almazroui et al., 2020). These observations are further explained by the fact that wind changes in the region favour the flow towards the west coast. This brings dry air from the Sahara region and prevents the storms coming from the ocean to hit the region. Further investigations on regional climatology using CMIP6 simulations are therefore needed to explain this discrepancy. Yet, the overall change of the precipitation might not be considered as significant nor robust. Moreover, the present work also shed light on an increase of precipitation during the summer time (JJA). Generally, simulations based on the CMIP6 indicate that an increase is expected, see for example (Cos et al., 2022). As opposed to simulations for which the CMIP5 were used, the trend is oriented towards a general decrease, see Tuel et al. (2021); Cos et al. (2022). **A similar pattern has also been revealed in the study by (Bichet et al., 2020). In their study, a precipitation decrease of 20% by 2030, 30% by 2040 and 50% by 2050 is predicted in the northernmost regions of Africa. These results are in good agreement with the findings of the present study.** The results in the current work show that the precipitation will decrease in the MAM and SON seasons in all scenarios except for a local region in the north. In this regard, studies conducted by (Lachgar et al., 2021) and (Tomaszkiewicz, 2021), to a limited extent, both in terms of the number of models and the spatial coverage, have predicted a decrease in the precipitation in these seasons. In addition, there is a consistency with results of many studies in the literature (Hamed et al., 2022; Du et al., 2022; Mesgari et al., 2022; Spinoni et al., 2020) with the increase in the annual precipitation in the Sahara region determined in this study. According to other studies from the literature and results of this present study, it is concluded that there is a common agreement about the southern part of Morocco, but there is no common consensus about the northern part of Morocco. In terms of seasonal variations, changes in DJF season give results contrary to previous studies but, there is a good agreement in other seasons. Thus, it is also expected that the precipitation patterns of the country will change significantly, and the amount of precipitation will be reduced to half, especially in areas other than the south of the country.

6 Conclusions

In the present study, a statistical downscaling method based on the ANN and multi-model ensemble is implemented over Morocco. The learning class of the ANN is developed using ground stations which allowed to both validate the downscaling and also to assess the best GCMs able to simulate the regional climate in Morocco. Next, using different climate scenarios, projections of the temperature and precipitation have been performed and spatio-temporal variability of different climate parameters have also been assessed. Results obtained for this analysis, confirm that Morocco is prone to high levels of variability at seasonal, annual and decadal scales. Overall, the temperature is expected to increase in the near future but also in the mid and far future and its increase is consistent throughout the seasons as well. The precipitation exhibits also a high level of variability and yet, some discrepancies are observed for the general trend of changes during winter and summer seasons compared to previous studies available in the literature, especially those using the CMIP5 simulations. This needs further investigation to understand the reasons behind these surprising changes. A careful analysis of the regional climatology is therefore needed to further understand these projections. In this study, the changes in annual and seasonal values of the precipitation and temperature under different scenarios reveal that Morocco is a vulnerable region regarding climate change. For this reason, studies on adaptation to climate change in the country should be implemented by decision-makers. Finally, it is suggested that the effects of these possible changes in the precipitation and temperature patterns on the country for drought should also be investigated for different scenarios.

Author contributions

Veysel Gumus: Conceptualization, Software, Writing - Original Draft, Formal analysis, **Nabil El Moçayd:** Writing - Original Draft, Validation, Resources, Data Curation, **Mehmet Seker:** Methodology, Formal analysis, Writing - Original Draft, **Mohammed Seaid:** Writing - Review & Editing, Validation, Visualization

Acknowledgments and funding

The authors greatly acknowledge Dr Moulay Driss Hasnaoui from the Moroccan Water Ministry and the Moroccan State Meteorological Service in Morocco for providing the meteorological data used in this study. The first author has been supported by The Scientific and Research Council of Turkey (TUBITAK) to conduct research under TUBITAK-2219-International Postdoctoral Research Fellowship Program for Turkish Citizens. The second author has been supported by OCP through the UMRP program. The support is gratefully acknowledged.

Data availability

The data underlying the results can be obtained from the corresponding author on a reasonable request.

Conflict of interest

The authors have no competing interests to declare that are relevant to the content of this paper.

References

Abbas, A., Ullah, S., Ullah, W., Waseem, M., Dou, X., Zhao, C., Karim, A., Zhu, J., Hagan, D.F.T., Bhatti, A.S., Ali, G., 2022. Evaluation and projection of precipitation in Pakistan using the coupled model intercomparison project phase 6 model simulations. International Journal of Climatology 42, 6665–6684.

Abdelmajid, S., Mukhtar, A., Baig, M.B., Reed, M.R., 2021. Climate change, agricultural policy and food security in Morocco, in: Emerging challenges to food production and security in Asia, Middle East, and Africa. Springer, pp. 171–196.

Ahmed, K., Shahid, S., Sachindra, D.A., Nawaz, N., Chung, E.S., 2019. Fidelity assessment of general circulation model simulated precipitation and temperature over Pakistan using a feature selection method. Journal of Hydrology 573, 281–298.

Almazroui, M., Saeed, F., Saeed, S., Nazrul Islam, M., Ismail, M., Klutse, N.A.B., Siddiqui, M.H., 2020. Projected change in temperature and precipitation over africa from CMIP6. Earth Systems and Environment 4, 455–475.

Babaousmail, H., Hou, R., Ayugi, B., Ojara, M., Ngoma, H., Karim, R., Rajasekar, A., Ongoma, V., 2021. Evaluation of the performance of CMIP6 models in reproducing rainfall patterns over north africa. Atmosphere 12.

Bi, D., Dix, M., Marsland, S., O'Farrell, S., Rashid, H., Uotila, P., Hirst, A., Kowalczyk, E., Golebiewski, M., Sullivan, A., Yan, H., Hannah, N., Franklin, C., Sun, Z., Vohralik, P., Watterson, I., Zhou, X., Fiedler, R., Collier, M., Ma, Y., Noonan, J., Stevens, L., Uhe, P., Zhu, H., Griffies, S., Hill, R., Harris, C., Puri, K., 2013. The ACCESS coupled model: Description, control climate and evaluation. Australian Meteorological and Oceanographic Journal 63, 41–64.

Bichet, A., Diedhiou, A., Hingray, B., Evin, G., Touré, N.E., Browne, K.N.A., Kouadio, K., 2020. Assessing uncertainties in the regional projections of precipitation in CORDEX-AFRICA. Climatic Change 162, 583–601.

Boucher, O., Servonnat, J., Albright, A.L., Aumont, O., Balkanski, Y., Bastrikov, V., Bekki, S., Bonnet, R., Bony, S., Bopp, L., Braconnot, P., Brockmann, P., Cadule, P., Caubel, A., Cheruy, F., Codron, F., Cozic, A., Cugnet, D., D'Andrea, F., Davini, P., de Lavergne, C., Denvil, S., Deshayes, J., Devilliers, M., Ducharne, A., Dufresne, J., Dupont, E., Éthé, C., Fairhead, L., Falletti, L., Flavoni, S., Foujols, M., Gardoll, S., Gastineau, G., Ghattas, J., Grandpeix, J., Guenet, B., Guez, L.E., Guilyardi, E., Guimberteau, M., Hauglustaine, D., Hourdin, F., Idelkadi, A., Joussaume, S., Kageyama, M., Khodri, M., Krinner, G., Lebas, N., Levavasseur, G., Lévy, C., Li, L., Lott, F., Lurton, T., Luyssaert, S., Madec, G., Madeleine, J., Maignan, F., Marchand, M., Marti, O., Mellul, L., Meurdesoif, Y., Mignot, J., Musat, I., Ottlé, C., Peylin, P., Planton, Y., Polcher, J., Rio, C., Rochetin, N., Rousset, C., Sepulchre, P., Sima, A., Swingedouw, D., Thiéblemont, R., Traore, A.K., Vancoppenolle, M., Vial, J., Vialard, J., Viovy, N., Vuichard, N., 2020. Presentation and evaluation of the IPSL-CM6A-LR climate model. Journal of Advances in Modeling Earth Systems 12.

Cao, J., Wang, B., Yang, Y.M., Ma, L., Li, J., Sun, B., Bao, Y., He, J., Zhou, X., Wu, L., 2018. The nuist earth system model (NESM) version 3: description and preliminary evaluation. Geoscientific Model Development 11, 2975–2993.

Carvalho, D., Cardoso Pereira, S., Rocha, A., 2021. Future surface temperatures over Europe according to CMIP6 climate projections: an analysis with original and bias-corrected data. Climatic Change 167.

Chaqdid, A., Tuel, A., El Fatimy, A., El Moçayd, N., 2023. Extreme rainfall events in morocco: Spatial dependence and climate drivers. Weather and Climate Extremes 40, 100556.

Cos, J., Doblas-Reyes, F., Jury, M., Marcos, R., Bretonnière, P.A., Samsó, M., 2022. The Mediterranean climate change hotspot in the CMIP5 and CMIP6 projections. Earth System Dynamics 13, 321–340.

Dey, A., Sahoo, D.P., Kumar, R., Remesan, R., 2022. A multimodel ensemble machine learning approach for CMIP6 climate model projections in an indian river basin. International Journal of Climatology 42, 9215–9236.

Du, Y., Wang, D., Zhu, J., Wang, D., Qi, X., Cai, J., 2022. Comprehensive assessment of CMIP5 and CMIP6 models in simulating and projecting precipitation over the global land. International Journal of Climatology 42, 6859–6875.

Dunne, J.P., Horowitz, L.W., Adcroft, A.J., Ginoux, P., Held, I.M., John, J.G., Krasting, J.P., Malyshev, S., Naik, V., Paulot, F., Shevliakova, E., Stock, C.A., Zadeh, N., Balaji, V., Blanton, C., Dunne, K.A., Dupuis, C., Durachta, J., Dussin, R., Gauthier, P.P.G., Griffies, S.M., Guo, H., Hallberg, R.W., Harrison, M., He, J., Hurlin, W., McHugh, C., Menzel, R., Milly, P.C.D., Nikonov, S., Paynter, D.J., Ploshay, J., Radhakrishnan, A., Rand, K., Reichl, B.G., Robinson, T., Schwarzkopf, D.M., Sentman, L.T., Underwood, S., Vahlenkamp, H., Winton, M., Wittenberg, A.T., Wyman, B., Zeng, Y., Zhao, M., 2020. The GFDL earth system model version 4.1 (GFDL-ESM 4.1): Overall coupled model description and simulation characteristics. Journal of Advances in Modeling Earth Systems 12.

El-Mahdy, M.E.S., El-Abd, W.A., Morsi, F.I., 2021. Forecasting lake evaporation under a changing climate with an integrated artificial neural network model: A case study lake Nasser, Egypt. Journal of African Earth Sciences 179.

El Moçayd, N., Kang, S., Eltahir, E.A., 2020. Climate change impacts on the water highway project in Morocco. Hydrology and Earth System Sciences 24, 1467–1483.

El Moçayd, N., Seaid, M., 2021. Data-driven polynomial chaos expansions for characterization of complex fluid rheology: Case study of phosphate slurry. Reliability Engineering & System Safety 216, 107923.

Gadouali, F., Semane, N., Muñoz, Á., Messouli, M., 2020. On the link between the madden-julian oscillation, Euro-Mediterranean weather regimes, and Morocco winter rainfall. Journal of Geophysical Research: Atmospheres 125, e2020JD032387.

Gao, X., Pal, J.S., Giorgi, F., 2006. Projected changes in mean and extreme precipitation over the Mediterranean region from a high resolution double nested rcm simulation. Geophysical Research Letters 33.

Guo, H., Bao, A., Chen, T., Zheng, G., Wang, Y., Jiang, L., De Maeyer, P., 2021. Assessment of CMIP6 in simulating precipitation over arid central asia. Atmospheric Research 252.

Gutjahr, O., Putrasahan, D., Lohmann, K., Jungclaus, J.H., von Storch, J.S., Brüggemann, N., Haak, H., Stössel, A., 2019. Max Planck institute earth system model (MPI-ESM1.2) for the high-resolution model intercomparison project (HighResMIP). Geoscientific Model Development 12, 3241–3281.

Habib, R.R., Zein, K.E., Ghanawi, J., 2010. Climate change and health research in the eastern Mediterranean region. EcoHealth 7, 156–175.

Hallegatte, S., 2009. Strategies to adapt to an uncertain climate change. Global environmental change 19, 240–247.

Hamed, M.M., Nashwan, M.S., Shiru, M.S., Shahid, S., 2022. Comparison between CMIP5 and CMIP6 models over MENA region using historical simulations and future projections. Sustainability 14.

Hosseini Baghanam, A., Norouzi, E., Nourani, V., 2022. Wavelet-based predictor screening for statistical downscaling of precipitation and temperature using the artificial neural network method. Hydrology Research 53, 385–406.

Iqbal, Z., Shahid, S., Ahmed, K., Ismail, T., Khan, N., Virk, Z.T., Johar, W., 2020. Evaluation of global climate models for precipitation projection in sub-Himalaya region of Pakistan. Atmospheric Research 245.

Kelley, M., Schmidt, G.A., Nazarenko, L.S., Bauer, S.E., Ruedy, R., Russell, G.L., Ackerman, A.S., Aleinov, I., Bauer, M., Bleck, R., Canuto, V., Cesana, G., Cheng, Y., Clune, T.L., Cook, B.I., Cruz, C.A., Del Genio, A.D., Elsaesser, G.S., Faluvegi, G., Kiang, N.Y., Kim, D., Lacis, A.A., Leboissetier, A., LeGrande, A.N., Lo, K.K., Marshall, J., Matthews, E.E., McDermid, S., Mezuman, K., Miller, R.L., Murray, L.T., Oinas, V., Orbe, C., García-Pando, C.P., Perlwitz, J.P., Puma, M.J., Rind, D., Romanou, A., Shindell, D.T., Sun, S., Tausnev, N., Tsigaridis, K., Tselioudis, G., Weng, E., Wu, J., Yao, M., 2020. GISS-E2.1: Configurations and climatology. Journal of Advances in Modeling Earth Systems 12.

Keskin, M.E., Terzi, O., 2006. Artificial neural network models of daily pan evaporation. Journal of Hydrologic Engineering 11, 65–70.

Khomsi, K., Najmi, H., Souhaili, Z., 2018. Co-occurrence of extreme ozone and heat waves in two cities from Morocco. Satellite Oceanography and Meteorology 3.

Knippertz, P., Christoph, M., Speth, P., 2003. Long-term precipitation variability in Morocco and the link to the large-scale circulation in recent and future climates. Meteorology and Atmospheric physics 83, 67–88.

Koch, J., Demirel, M.C., Stisen, S., 2018. The spatial efficiency metric (SPAEF): Multiple-component evaluation of spatial patterns for optimization of hydrological models. Geoscientific Model Development 11, 1873–1886.

Kulyamin, D.V., Volodin, E.M., 2018. INM RAS coupled atmosphere–ionosphere general circulation model INMAIM (0–130 km). Russian Journal of Numerical Analysis and Mathematical Modelling 33, 351–357.

Lachgar, R., Badri, W., Chlaida, M., 2021. Assessment of future changes in downscaled temperature and precipitation over the Casablanca-Settat region (Morocco). Modeling Earth Systems and Environment 8, 2123–2133.

Li, L., Yu, Y., Tang, Y., Lin, P., Xie, J., Song, M., Dong, L., Zhou, T., Liu, L., Wang, L., Pu, Y., Chen, X., Chen, L., Xie, Z., Liu, H., Zhang, L., Huang, X., Feng, T., Zheng, W., Xia, K., Liu, H., Liu, J., Wang, Y., Wang, L., Jia, B., Xie, F., Wang, B., Zhao, S., Yu, Z., Zhao, B., Wei, J., 2020. The flexible global ocean-atmosphere-land system model grid-point version 3 (FGOALS-g3): Description and evaluation. Journal of Advances in Modeling Earth Systems 12.

Li, W., Jiang, Z., Xu, J., Li, L., 2015. Extreme precipitation indices over China in CMIP5 models. Part I: Model evaluation. Journal of Climate 28, 8603–8619.

Majdi, F., Hosseini, S.A., Karbalaee, A., Kaseri, M., Marjanian, S., 2022. Future projection of precipitation and temperature changes in the middle east and north africa (MENA) region based on CMIP6. Theoretical and Applied Climatology 147, 1249–1262.

Manzanas, R., Brands, S., San-Martín, D., Lucero, A., Limbo, C., Gutiérrez, J., 2015. Statistical downscaling in the tropics can be sensitive to reanalysis choice: a case study for precipitation in the philippines. Journal of Climate 28, 4171–4184.

Maqsood, J., Farooque, A.A., Abbas, F., Esau, T., Wang, X., Acharya, B., Afzaal, H., 2022. Application of artificial neural networks to project reference evapotranspiration under climate change scenarios. Water Resources Management 36, 835–851.

Marquardt, D.W., 1963. An algorithm for least-squares estimation of nonlinear parameters. Journal of the Society for Industrial and Applied Mathematics 11, 431–441.

Meinshausen, M., Nicholls, Z.R.J., Lewis, J., Gidden, M.J., Vogel, E., Freund, M., Beyerle, U., Gessner, C., Nauels, A., Bauer, N., Canadell, J.G., Daniel, J.S., John, A., Krummel, P.B., Luderer, G., Meinshausen, N., Montzka, S.A., Rayner, P.J., Reimann, S., Smith, S.J., van den Berg, M., Velders, G.J.M., Vollmer, M.K., Wang, R.H.J., 2020. The shared socio-economic pathway (SSP) greenhouse gas concentrations and their extensions to 2500. Geoscientific Model Development 13, 3571–3605.

Mesgari, E., Hosseini, S.A., Hemmesy, M.S., Houshyar, M., Partoo, L.G., 2022. Assessment of CMIP6 models' performances and projection of precipitation based on ssp scenarios over the MENAp region. Journal of Water and Climate Change 13, 3607–3619.

Nash, J.E., Sutcliffe, J.V., 1970. River flow forecasting through conceptual models Part I - A discussion of principles. Journal of Hydrology 10, 282–290.

Nashwan, M.S., Shahid, S., 2022. Future precipitation changes in Egypt under the 1.5 and 2.0 ° c global warming goals using CMIP6 multimodel ensemble. Atmospheric Research 265.

Okkan, U., Kirdemir, U., 2016. Downscaling of monthly precipitation using cmip5 climate models operated under rcps. Meteorological Applications 23, 514–528.

O'Neill, B.C., Kriegler, E., Riahi, K., Ebi, K.L., Hallegatte, S., Carter, T.R., Mathur, R., van Vuuren, D.P., 2013. A new scenario framework for climate change research: the concept of shared socioeconomic pathways. Climatic Change 122, 387–400.

Raulino, J.B.S., Silveira, C.S., Lima Neto, I.E., 2021. Assessment of climate change impacts on hydrology and water quality of large semi-arid reservoirs in Brazil. Hydrological Sciences Journal 66, 1321–1336.

Riahi, K., van Vuuren, D.P., Kriegler, E., Edmonds, J., O'Neill, B.C., Fujimori, S., Bauer, N., Calvin, K., Dellink, R., Fricko, O., Lutz, W., Popp, A., Cuaresma, J.C., Kc, S., Leimbach, M., Jiang, L., Kram, T., Rao, S., Emmerling, J., Ebi, K., Hasegawa, T., Havlik, P., Humpenöder, F., Da Silva, L.A., Smith, S., Stehfest, E., Bosetti, V., Eom, J., Gernaat, D., Masui, T., Rogelj, J., Strefler, J., Drouet, L., Krey, V., Luderer, G., Harmsen, M., Takahashi, K., Baumstark, L., Doelman, J.C., Kainuma, M., Klimont, Z., Marangoni, G., Lotze-Campen, H., Obersteiner, M., Tabeau, A., Tavoni, M., 2017. The shared socioeconomic pathways and their energy, land use, and greenhouse gas emissions implications: An overview. Global Environmental Change 42, 153–168.

Rivera, J.A., Arnould, G., 2020. Evaluation of the ability of CMIP6 models to simulate precipitation over southwestern south america: Climatic features and long-term trends (1901–2014). Atmospheric Research 241.

Ruffault, J., Martin-StPaul, N.K., Duffet, C., Goge, F., Mouillot, F., 2014. Projecting future drought in Mediterranean forests: Bias correction of climate models matters! Theoretical and Applied Climatology 117, 113–122.

Rumelhart, D.E., McClelland, J.L., Group, P.R., 1988. Parallel distributed processing. volume 1. MIT Press, Cambridge.

Sachindra, D., Ahmed, K., Rashid, M.M., Shahid, S., Perera, B., 2018. Statistical downscaling of precipitation using machine learning techniques. Atmospheric research 212, 240–258.

Satour, N., Raji, O., El Moçayd, N., Kacimi, I., Kassou, N., 2021. Spatialized flood resilience measurement in rapidly urbanized coastal areas with a complex semi-arid environment in northern Morocco. Natural Hazards and Earth System Sciences 21, 1101–1118.

Schilling, J., Freier, K.P., Hertig, E., Scheffran, J., 2012. Climate change, vulnerability and adaptation in north africa with focus on Morocco. Agriculture, Ecosystems & Environment 156, 12–26.

Seker, M., Gumus, V., 2022. Projection of temperature and precipitation in the Mediterranean region through multi-model ensemble from CMIP6. Atmospheric Research 280.

Spinoni, J., Barbosa, P., Bucchignani, E., Cassano, J., Cavazos, T., Christensen, J.H., Christensen, O.B., Coppola, E., Evans, J., Geyer, B., Giorgi, F., Hadjinicolaou, P., Jacob, D., Katzfey, J., Koenigk, T., Laprise, R., Lennard, C.J., Kurnaz, M.L., Li, D., Llopart, M., McCormick, N., Naumann, G., Nikulin, G., Ozturk, T., Panitz, H.J., Porfirio da Rocha, R., Rockel, B., Solman, S.A., Syktus, J., Tangang, F., Teichmann, C., Vautard, R., Vogt, J.V., Winger, K., Zittis, G., Dosio, A., 2020. Future global meteorological drought hot spots: A study based on cordex data. Journal of Climate 33, 3635–3661.

Sudheer, K.P., Gosain, A.K., Mohana Rangan, D., Saheb, S.M., 2002. Modelling evaporation using an artificial neural network algorithm. Hydrological Processes 16, 3189–3202.

Svozil, D., Kvasnicka, V., Pospichal, J., 1997. Introduction to multi-layer feed-forward neural networks. Chemometrics and Intelligent Laboratory Systems 39, 43–62.

Swart, N.C., Cole, J.N.S., Kharin, V.V., Lazare, M., Scinocca, J.F., Gillett, N.P., Anstey, J., Arora, V., Christian, J.R., Hanna, S., Jiao, Y., Lee, W.G., Majaess, F., Saenko, O.A., Seiler, C., Seinen, C., Shao, A., Sigmond, M., Solheim, L., von Salzen, K., Yang, D., Winter, B., 2019. The canadian earth system model version 5 (canESM5.0.3). Geoscientific Model Development 12, 4823–4873.

Séférian, R., Nabat, P., Michou, M., Saint-Martin, D., Voldoire, A., Colin, J., Decharme, B., Delire, C., Berthet, S., Chevallier, M., Sénési, S., Franchisteguy, L., Vial, J., Mallet, M., Joetzjer, E., Geoffroy, O., Guérémy, J., Moine, M., Msadek, R., Ribes, A., Rocher, M., Roehrig, R., Salas-y-Mélia, D., Sanchez, E., Terray, L., Valcke, S., Waldman, R., Aumont, O., Bopp, L., Deshayes, J., Éthé, C., Madec, G., 2019. Evaluation of cnrm earth system model, cnrm-ESM2-1: Role of earth system processes in present-day and future climate. Journal of Advances in Modeling Earth Systems 11, 4182–4227.

Tatebe, H., Ogura, T., Nitta, T., Komuro, Y., Ogochi, K., Takemura, T., Sudo, K., Sekiguchi, M., Abe, M., Saito, F., Chikira, M., Watanabe, S., Mori, M., Hirota, N., Kawatani, Y., Mochizuki, T., Yoshimura, K., Takata, K., O'Ishi, R., Yamazaki, D., Suzuki, T., Kurogi, M., Kataoka, T., Watanabe, M., Kimoto, M., 2019. Description and basic evaluation of simulated mean state, internal variability, and climate sensitivity in miroc6. Geoscientific Model Development 12, 2727–2765.

Tomaszkiewicz, M.A., 2021. Future seasonal drought conditions over the cordex-MENA/arab domain. Atmosphere 12.

Tramblay, Y., Badi, W., Driouech, F., El Adlouni, S., Neppel, L., Servat, E., 2012.

Climate change impacts on extreme precipitation in Morocco. Global and Planetary change 82, 104–114.

Tramblay, Y., Ruelland, D., Somot, S., Bouaicha, R., Servat, E., 2013. High-resolution med-cordex regional climate model simulations for hydrological impact studies: A first evaluation of the ALADIN-climate model in Morocco. Hydrology and Earth System Sciences 17, 3721–3739.

Tuel, A., El Moçayd, N., 2023. Evaluating extreme precipitation in gridded datasets with a novel station database in morocco. Stochastic Environmental Research and Risk Assessment , 1–13.

Tuel, A., El Moçayd, N., Hasnaoui, M.D., Eltahir, E.A.B., 2022. Future projections of high atlas snowpack and runoff under climate change. Hydrology and Earth System Sciences 26, 571–588.

Tuel, A., Eltahir, E.A., 2020. Why is the Mediterranean a climate change hot spot? Journal of Climate 33, 5829–5843.

Tuel, A., Kang, S., Eltahir, E.A., 2021. Understanding climate change over the southwestern Mediterranean using high-resolution simulations. Climate Dynamics 56, 985–1001.

Voldoire, A., Saint-Martin, D., Sénési, S., Decharme, B., Alias, A., Chevallier, M., Colin, J., Guérémy, J.F., Michou, M., Moine, M.P., Nabat, P., Roehrig, R., Salas y Mélia, D., Séférian, R., Valcke, S., Beau, I., Belamari, S., Berthet, S., Cassou, C., Cattiaux, J., Deshayes, J., Douville, H., Ethé, C., Franchistéguy, L., Geoffroy, O., Lévy, C., Madec, G., Meurdesoif, Y., Msadek, R., Ribes, A., Sanchez-Gomez, E., Terray, L., Waldman, R., 2019. Evaluation of CMIP6 deck experiments with CNRM-CM6-1. Journal of Advances in Modeling Earth Systems 11, 2177–2213.

Willmott, C.J., 1981. On the validation of models. Physical Geography 2, 184–194.

Wu, C.H., Huang, G.R., Yu, H.J., 2015. Prediction of extreme floods based on CMIP5 climate models: A case study in the Beijiang river basin, south China. Hydrology and Earth System Sciences 19, 1385–1399.

Xu, K., Xu, B., Ju, J., Wu, C., Dai, H., Hu, B.X., 2019. Projection and uncertainty of precipitation extremes in the CMIP5 multimodel ensembles over nine major basins in China. Atmospheric Research 226, 122–137.

You, Q., Zhang, Y., Chen, C., Ge, J., Adnan, M., 2018. Evaluation of downscaled CMIP5 coupled with VIC model for flash drought simulation in a humid subtropical basin, China. Journal of Climate 31, 1075–1090.

Yukimoto, S., Kawai, H., Koshiro, T., Oshima, N., Yoshida, K., Urakawa, S., Tsujino, H., Deushi, M., Tanaka, T., Hosaka, M., Yabu, S., Yoshimura, H., Shindo, E., Mizuta, R., Obata, A., Adachi, Y., Ishii, M., 2019. The meteorological research institute earth system model version 2.0, MRI-ESM2.0: Description and basic evaluation of the physical component. Journal of the Meteorological Society of Japan. Ser. II 97, 931–965.

Zkhiri, W., Tramblay, Y., Hanich, L., Jarlan, L., Ruelland, D., 2019. Spatiotemporal characterization of current and future droughts in the high atlas basins (Morocco). Theoretical and Applied Climatology 135, 593–605.